University of Groningen

The mitochondrial peptidase, neurolysin, regulates respiratory chain supercomplex formation and is necessary for AML viability

Mirali, Sara; Botham, Aaron; Voisin, Veronique; Xu, Changjiang; St-Germain, Jonathan; Sharon, David; Hoff, Fieke W; Qiu, Yihua; Hurren, Rose; Gronda, Marcela

IMPORTANT NOTE: You are advised to consult the publisher's version (publisher's PDF) if you wish to cite from it. Please check the document version below.

Document Version
Publisher's PDF, also known as Version of record

[Link to publication in University of Groningen/UMCG research database](#)

CANCER

The mitochondrial peptidase, neurolysin, regulates respiratory chain supercomplex formation and is necessary for AML viability

Sara Mirali[1,2], Aaron Botham[1,3], Veronique Voisin[4], Changjiang Xu[4], Jonathan St-Germain[1], David Sharon[1], Fieke W. Hoff[5,6], Yihua Qiu[6], Rose Hurren[1], Marcela Gronda[1], Yulia Jitkova[1], Boaz Nachmias[1], Neil MacLean[1], Xiaoming Wang[1], Andrea Arruda[1], Mark D. Minden[1,2,3], Terzah M. Horton[7], Steven M. Kornblau[6], Steven M. Chan[1,3], Gary D. Bader[4,8], Brian Raught[1,3], Aaron D. Schimmer[1,2,3]*

Neurolysin (NLN) is a zinc metallopeptidase whose mitochondrial function is unclear. We found that NLN was overexpressed in almost half of patients with acute myeloid leukemia (AML), and inhibition of NLN was selectively cytotoxic to AML cells and stem cells while sparing normal hematopoietic cells. Mechanistically, NLN interacted with the mitochondrial respiratory chain. Genetic and chemical inhibition of NLN impaired oxidative metabolism and disrupted the formation of respiratory chain supercomplexes (RCS). Furthermore, NLN interacted with the known RCS regulator, LETM1, and inhibition of NLN disrupted LETM1 complex formation. RCS were increased in patients with AML and positively correlated with NLN expression. These findings demonstrate that inhibiting RCS formation selectively targets AML cells and stem cells and highlights the therapeutic potential of pharmacologically targeting NLN in AML.

INTRODUCTION

Acute myeloid leukemia (AML) cells and stem cells have distinctive mitochondrial properties with increased reliance on oxidative phosphorylation (1–4). Mitochondrial functions, including oxidative phosphorylation, are tightly regulated by protein quality control systems, including mitochondrial proteases. We previously found that select mitochondrial proteases are important for AML viability (1). Mitochondrial proteases maintain the integrity of mitochondrial pathways such as mitochondrial dynamics, metabolism, and apoptosis (5). For example, the mitochondrial matrix protease, caseinolytic protease P (ClpP), degrades damaged and misfolded respiratory chain proteins to maintain the integrity of the respiratory chain (1).

Neurolysin (NLN) is a zinc metallopeptidase that is localized to the mitochondria and is also secreted into the circulation. In the circulation, NLN cleaves vasoactive peptides such as neurotensin and bradykinin to regulate physiological processes such as blood pressure (6–10). Despite this reported function, NLN knockout (KO) mice are viable with normal blood pressure, suggesting that NLN's effects on vasoactive peptides are redundant in vivo. However, NLN KO mice demonstrate mild metabolic defects with reduced mitochondrial oxidative activity in their muscle fibers (11). Although the role of NLN in the circulation has been well characterized, its mitochondrial function is largely unknown. Initially, NLN was thought

to localize to the mitochondrial intermembrane space, but more recent work localized NLN to the mitochondrial matrix (12–14). However, the function of NLN in the matrix is unclear.

We determined that NLN is necessary for the formation of respiratory complexes and higher order supercomplexes in the mitochondria. Respiratory chain complexes I, III, and IV assemble into higher-order quaternary structures termed respiratory chain supercomplexes (RCS). RCS enhance electron transport and mitochondrial respiration (15–17). We showed that NLN expression positively correlates with the amount of RCS in primary AML samples. Moreover, NLN is necessary for the growth and viability of AML cells and stem cells in vitro and in vivo. Thus, we identified a role for NLN in RCS formation and highlight a biological vulnerability in the mitochondria of AML.

RESULTS

NLN is necessary for the growth of leukemic cells and progenitors

We previously identified the mitochondrial peptidase NLN as a top hit in a short hairpin RNA (shRNA) screen to identify potential biological vulnerabilities in the mitochondrial proteome of AML cells (1). NLN's mitochondrial function is not well understood, and its role in AML has not been previously reported. We initiated our study into the role of NLN in leukemia by analyzing *NLN* gene expression in AML cells and stem cells. In a database of 536 AML and 73 normal bone marrow samples, *NLN* was overexpressed in 41% of AML samples (Fig. 1A, fig. S1A, and data file S1). *NLN* was equally expressed in the CD34$^+$ and CD34$^-$ AML cell populations, as well as in the leukemic stem cell (LSC)$^+$ and LSC$^-$ fractions, which were defined by their ability to differentiate and self-renew in vivo (fig. S1, B and C) (18). *NLN* expression correlated with *RUNX1*, *FLT3*, *NPM1*, and *ASXL1* mutations (table S1). We confirmed the overexpression of NLN in primary AML cells compared to normal hematopoietic cells by immunoblotting (Fig. 1B and fig. S1, D and E).

[1]Princess Margaret Cancer Centre, Toronto, Ontario M5G 1L7, Canada. [2]Institute of Medical Science, University of Toronto, Toronto M5S 1A8, Ontario, Canada. [3]Department of Medical Biophysics, University of Toronto, Toronto M5G 1L7, Ontario, Canada. [4]Donnelly Centre for Cellular and Biomolecular Research, Toronto, Ontario M5S 3E1, Canada. [5]Department of Pediatric Oncology/Hematology, University Medical Center Groningen, Groningen 9700 RB, Netherlands. [6]Department of Leukemia, The University of Texas MD Anderson Cancer Center, Houston, TX 77030, USA. [7]Texas Children's Cancer and Hematology Centers, Baylor College of Medicine, Houston, TX 77030, USA. [8]Department of Molecular Genetics, University of Toronto, Toronto M5S 1A8, Ontario, Canada.
*Corresponding author. Email: aaron.schimmer@uhn.ca

Fig. 1. Genetic knockdown of *NLN* reduces the growth of leukemic cells and progenitors. (**A**) Expression pattern and hierarchical clustering of microarray data from 536 primary human AML and 73 normal bone marrow samples for *NLN* expression. The four main AML *NLN* expression clusters were designated as 1, 2, 3, and 4. A whisker boxplot displays the *NLN* z-score normalized gene expression values for each sample in each cluster through their quartiles. The midline represents the median value for each group. One-way ANOVA was applied to test the significance of the differences in the mean expression values between the groups. Pairwise *t* tests were applied between each AML cluster and the normal data. Each *t* test was significant at $P < 2 \times 10^{-16}$. (**B**) NLN expression was assessed in isolated mitochondria from primary AML samples and normal hematopoietic cells. NLN and SDHA were analyzed by immunoblotting. (**C** to **E**) Knockdown of NLN in OCI-AML2 (C), NB4 (D), and TEX (E) cells was assessed by immunoblotting 8 days after transducing cells with shRNA targeting *NLN* or control sequences. Membranes were immunoblotted with antibodies against NLN and actin or GAPDH. (**F** to **H**) Viable cell counts of OCI-AML2 (F), NB4 (G), and TEX (H) cells seeded 4 days after transducing cells with shRNA targeting *NLN* or control sequences. Data points represent mean viable cell counts ± SD of a representative experiment from $N = 3$ biological replicates. (**I** and **J**) Clonogenic growth of OCI-AML2 (I) and NB4 (J) cells transduced with shRNA targeting *NLN* or control sequences. Means ± SEM colony counts are shown from $N = 2$ biological replicates. ****$P \leq 0.0001$ by one-way ANOVA and Dunnett's post hoc test. CFU, colony-forming units. (**K**) Equal numbers of viable TEX cells (2×10^5) transduced with shRNA targeting *NLN* or control sequences were injected into the right femur of sublethally irradiated immunodeficient mice. Six weeks after injection, mice were euthanized, and the percentage of human CD45$^+$ cells in the noninjected femur was determined by flow cytometry ($n = 10$ mice per group). Bar represents mean engraftment. **$P \leq 0.01$ by Student's *t* test.

Mirali *et al.*, *Sci. Transl. Med.* **12**, eaaz8264 (2020)   8 April 2020

2 of 16
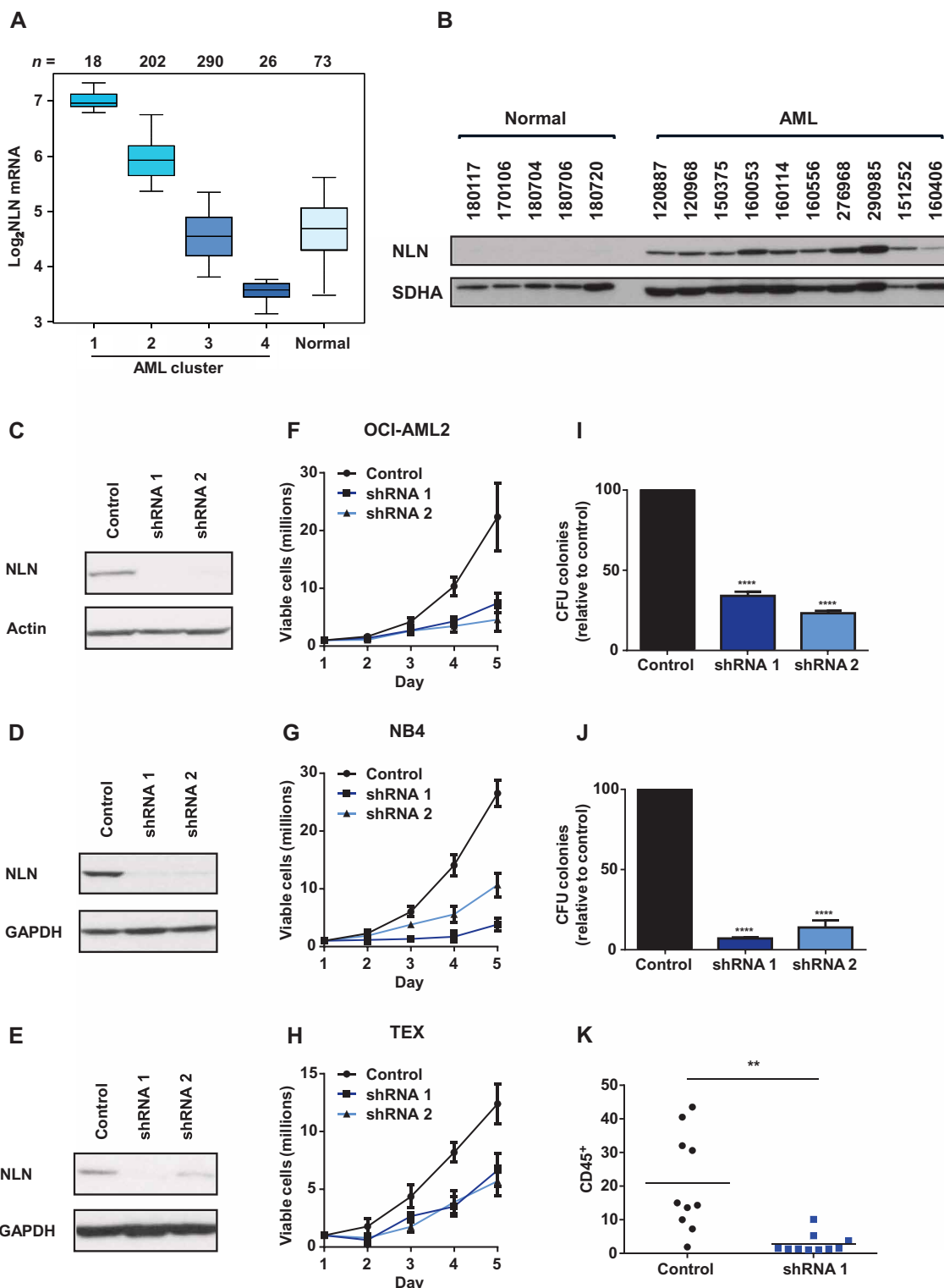
We assessed whether NLN is necessary for the growth and viability of AML cells. OCI-AML2, NB4, TEX, and MV4-11 leukemia cells were transduced with shRNA targeting *NLN* or control sequences. Target knockdown was confirmed by immunoblotting (Fig. 1, C to E, and fig. S1F). *NLN* knockdown did not affect the expression of the closely related cytoplasmic peptidase, thimet oligopeptidase, THOP1 (fig. S1G). *NLN* knockdown reduced the growth and viability of OCI-AML2, NB4, TEX, and MV4-11 cells (Fig. 1, F to H, and fig. S1, H to L). Knockdown of *NLN* also reduced the clonogenic growth of AML cells (Fig. 1, I and J). To further test the effects of NLN on leukemia-initiating cells in vivo, we evaluated *NLN* knockdown in TEX cells, which have properties of LSCs, including hierarchal organization and self-renewal (19). Knockdown of *NLN* in TEX cells reduced engraftment into the marrow of immunodeficient mice (Fig. 1K and fig. S1M).

NLN interacts with the respiratory chain and regulates oxidative metabolism

To understand the mitochondrial function of NLN, we used proximity-dependent biotin labeling (BioID) coupled with mass spectrometry (MS) to identify the proteins that interact with NLN. We induced expression of Flag-BirA*-NLN in Flp-In T-REx human embryonic kidney (HEK) 293 cells and identified interacting proteins by MS. Interacting proteins were compared to Flag-BirA* and the known mitochondrial matrix protease, ClpP. From our BioID screen, we identified 86 proteins that preferentially interacted with NLN over the Flag-BirA* control, of which 72 localized to the mitochondria. Of these 72 mitochondrial proteins, 32 preferentially interacted with NLN over ClpP (data file S2). NLN's interactors were enriched for functions including respiratory electron transport, mitochondrion organization, and respiratory chain complex assembly (Fig. 2, A and B).

Because NLN interacted with respiratory chain complex proteins, we investigated the effects of *NLN* knockdown on oxidative phosphorylation. Knockdown of *NLN* decreased oxygen consumption rates (OCRs) (Fig. 2, C to E) and disrupted the formation of mitochondrial cristae (fig. S2A) in AML cells. However, knockdown of *NLN* did not alter the amounts of complex I, II, III, IV, or V subunits (Fig. 2, F and G, and fig. S2B). In addition, no changes in mitochondrial membrane potential, mitochondrial mass, or reactive oxygen species (ROS) were observed (fig. S2, C to F).

NLN knockdown impairs RCS formation

To understand how NLN affects oxidative phosphorylation, we examined the formation of respiratory chain complexes and supercomplexes. Respiratory chain complexes I, III, and IV assemble into large higher-order quaternary structures called RCS, which promote efficient oxidative metabolism (Fig. 3A). *NLN* knockdown impaired RCS formation in T-REx HEK293, NB4, and OCI-AML2 cells (Fig. 3, B to D, and fig. S3, A to C). In contrast, there was little to no effect on the assembly of respiratory chain complex II, which does not participate in supercomplex formation. The effects of *NLN* knockdown on RCS were independent of changes in amounts of the master cristae regulator, OPA1 (fig. S3D). Overexpressing wild-type shRNA-resistant *NLN* reversed the effects of *NLN* knockdown on supercomplex formation (Fig. 3E and fig. S3, E and F).

The effects of NLN on RCS formation stand in contrast to the effects of another mitochondrial matrix protease, ClpP. ClpP is activated by the mitochondrial chaperone ClpX (caseinolytic mito-chondrial matrix peptidase chaperone subunit X) to form ClpXP. *NLN* knockdown inhibited the formation of RCS but did not affect individual complex subunits. In contrast, ClpXP not only impaired RCS assembly (fig. S4A) but also degraded individual subunits of respiratory complexes I, III, and IV (fig. S4B).

To further investigate the requirement for NLN and respiratory supercomplexes in oxidative metabolism in AML, we analyzed NLN and RCS under hypoxia and near anoxia (1 and 0.2% oxygen). Under these hypoxic conditions, the amounts of individual complex subunits were unchanged. However, RCS assembly was reduced, and the amounts of NLN protein and mRNA were decreased (Fig. 3, F and G, and fig. S5, A to D). Moreover, under near anoxic conditions, NLN was not necessary for the growth of AML cells (Fig. 3H).

RCS assembly is enhanced in a subset of patients with AML and correlates with NLN expression

To further investigate the importance of RCS in AML, we analyzed RCS in primary AML patient samples and normal hematopoietic cells. RCS assembly was increased in a subset of AML patient samples compared to normal hematopoietic cells (Fig. 4A). Increased amounts of RCS positively correlated with increased NLN expression (Fig. 4B) but did not correlate with the amount of individual respiratory chain complex subunits (fig. S6, A and B). Collectively, these data suggest that RCS assembly is increased in a subset of AML patient samples and is correlated with NLN expression.

Inhibition of NLN reduces LETM1 complex assembly

To investigate how NLN may be regulating RCS assembly, we analyzed our BioID results. Among the top mitochondrial interactors with NLN was LETM1 (leucine zipper EF-hand containing transmembrane protein 1) (Fig. 5A). LETM1 is a known regulator of RCS formation (20). LETM1 forms two multiprotein complexes, termed the minor and major complexes. To investigate the role of LETM1 in oxidative metabolism in AML, we assessed LETM1 under hypoxia and near anoxia. Assembly of the minor and major complexes of LETM1 was impaired under hypoxia, but the amount of total LETM1 protein was only slightly reduced (fig. S7, A to D). Knockdown of *NLN* in AML cells reduced the formation of the minor and major LETM1 complexes, as assessed by nondenaturing gels, but only slightly changed total amounts of LETM1 protein (Fig. 5, B and C, and fig. S8, A to D). LETM1 was also reported to regulate mitochondrial calcium (21), but *NLN* knockdown did not alter cellular or mitochondrial calcium (fig. S8, E and F).

To further test whether RCS formation is necessary for oxidative phosphorylation and growth in AML, we knocked down *LETM1*. We also knocked down *BCS1L*, a known component of the LETM1 major complex (20) and an NLN interactor in our BioID screen. Knockdown of *LETM1* and *BCS1L* decreased basal and maximal OCR and reduced the growth of AML cells (Fig. 5, D to K, and fig. S8, G and H).

Chemical inhibition of NLN impairs supercomplex formation and targets primary AML cells and stem cells

3-[(2S)-1-[(3R)-3-(2-Chlorophenyl)-2-(2-fluorophenyl)pyrazolidin-1-yl]-1-oxopropan-2-yl]-1-(adamantan-2-yl)urea (R2) is an inhibitor of NLN (22), but its anticancer effects have not been previously reported. We assessed the effects of R2 on oxidative phosphorylation and RCS formation. Similar to genetic knockdown of *NLN*, chemical inhibition of NLN did not affect individual complex subunits but

Fig. 2. NLN interacts with the respiratory chain and NLN knockdown impairs oxidative metabolism. (**A**) Top Gene Ontology terms in the NLN interaction network. (**B**) List of proteins that interacted with NLN, as determined by proximity-dependent biotin labeling (BioID) coupled with mass spectrometry (MS). (**C**) Effects of *NLN* knockdown on oxidative metabolism in NB4 cells. Data points represent means ± SD, *n* = 5 technical replicates per group. (**D** and **E**) Effects of *NLN* knockdown on relative basal oxygen consumption in NB4 (D) and OCI-AML2 (E) cells. Values are shown as relative OCR compared to control shRNA. Means ± SD OCR values are shown, *n* = 5 to 10 technical replicates. ****$P \leq 0.0001$ by one-way ANOVA and Dunnett's post hoc test. (**F** and **G**) Lysates were collected from OCI-AML2 (F) and NB4 (G) cells 7 days after transduction with shRNA targeting *NLN* or a control sequence. NDUFA9 (complex I), SDHA (complex II), UQCRC2 (complex III), MTCO1 (complex IV), ATP5B (complex V), tubulin, GAPDH, and actin were measured by immunoblotting.
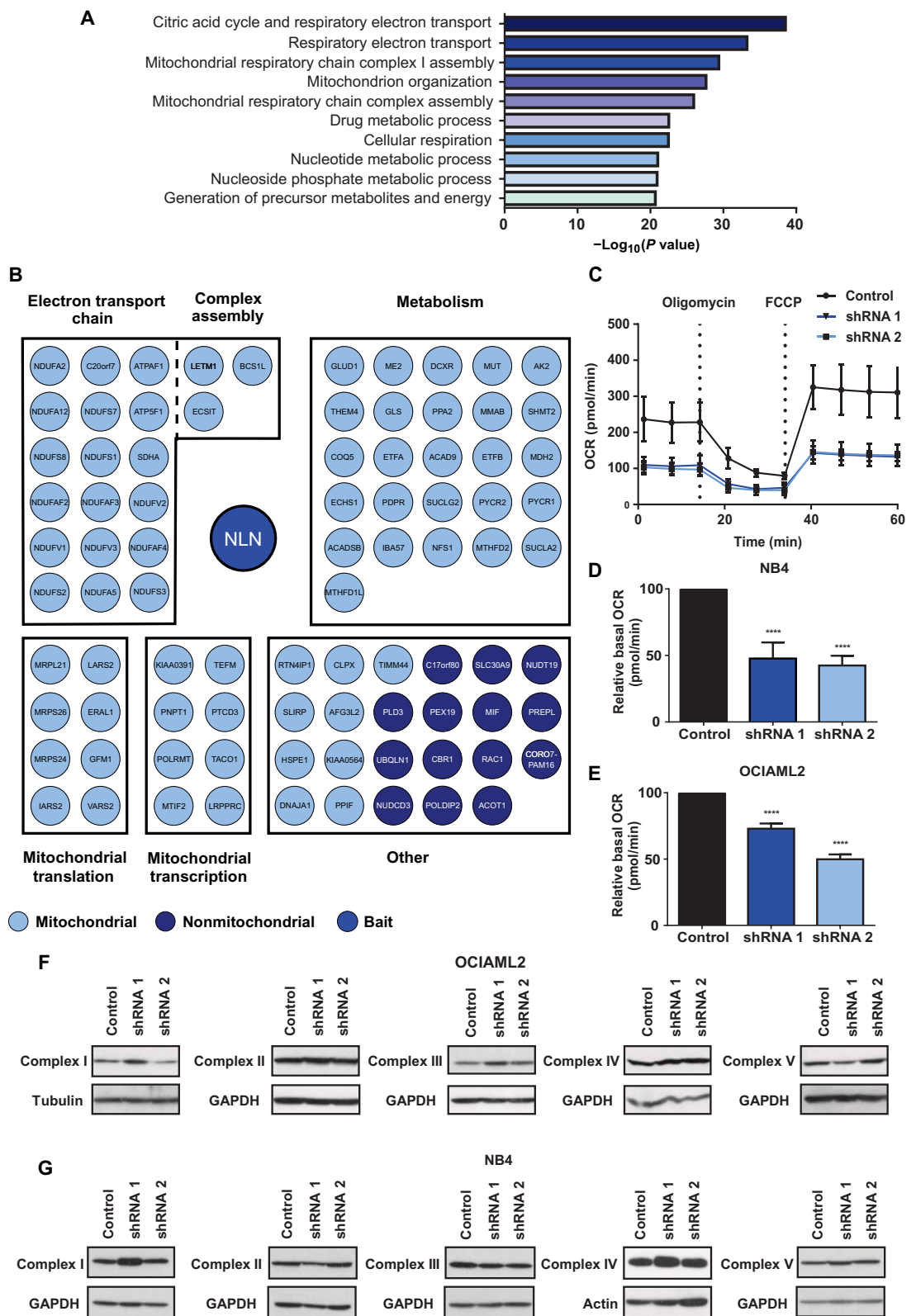
did impair complex and RCS formation in OCI-AML2 and NB4 cells (Fig. 6, A and B, and fig. S9A). Inhibition of NLN with R2 also decreased RCS formation in the 8227 primary AML culture model (*23*) and in primary AML cells (Fig. 6, C and D, and fig. S9, B and C).

Similar to the genetic knockdown of *NLN*, inhibition of NLN with R2 reduced the formation of LETM1 minor and major complexes with only slight changes in the total amount of LETM1 protein (Fig. 6E, and fig. S10, A to F). R2 also reduced the basal and maximal OCR in OCI-AML2 and 8227 cells (Fig. 6, F and G).

Inhibiting NLN with R2 reduced the growth and viability of AML cell lines (OCI-AML2, NB4, MV4-11, and TEX) (fig. S11A), as well as the primary AML culture models 8227 and 130578 (fig.

S11, B and C). Moreover, R2 treatment reduced the viability of functionally defined stem cells (defined by their ability to differentiate and self-renew in vitro) that reside in the CD34⁺CD38⁻

Mirali *et al.*, *Sci. Transl. Med.* **12**, eaaz8264 (2020)   8 April 2020

4 of 16

Fig. 3. NLN knockdown impairs RCS formation. (**A**) Proposed models for the organization of respiratory chain complexes. The traditional model postulates that each complex is independent of the others, and electron transfer depends on the random collision between complexes and electron carriers (top). Recent studies have found that respiratory complexes organize into large macromolecular structures called RCS (bottom). (**B** to **D**) Mitochondrial fractions were collected 7 days after Flp-In T-REx HEK293 (B), NB4 (C), and OCI-AML2 (D) cells were transduced with shRNA targeting *NLN* or control sequences. Isolated mitochondria were solubilized with digitonin and analyzed by BN-PAGE with antibodies against NDUFA9 (complex I), SDHA (complex II), UQCRC2 (complex III), and MTCO1 (complex IV). Representative immunoblots of $n = 2$ to 3 biological replicates. (**E**) OCI-AML2 cells overexpressing an empty vector (EV) or *NLN* were transduced with shRNA targeting the 3′ untranslated region (UTR) of *NLN* or a control sequence. Isolated mitochondria were solubilized with digitonin and analyzed by BN-PAGE with antibodies against NDUFA9 (complex I), SDHA (complex II), UQCRC2 (complex III), and MTCO1 (complex IV). Representative immunoblot of $n = 2$ biological replicates. (**F**) Mitochondrial fractions were collected after OCI-AML2 cells were incubated at 20, 1, or 0.2% O_2 for 48 hours. NLN, NDUFA9 (complex I), SDHA (complex II), UQCRC2 (complex III), and COXIV (complex IV) were measured by immunoblotting. Representative immunoblot of $n = 2$ biological replicates. (**G**) Mitochondrial fractions were collected after OCI-AML2 cells were incubated at 20, 1, or 0.2% O_2 for 48 hours. Isolated mitochondria were solubilized with digitonin. Complex and RCS assembly was measured by BN-PAGE with antibodies against NDUFA9 (complex I), SDHA (complex II), UQCRC2 (complex III), and MTCO1 (complex IV). Representative immunoblot of $n = 2$ biological replicates. (**H**) OCI-AML2 cells were transduced with shRNA targeting *NLN* or control sequences. Cells were incubated at 20, 1, or 0.2% O_2 and counted daily for 5 days by trypan blue exclusion staining. Data are shown as the mean area under the growth curve relative to control shRNA ± SD. Data points represent mean viable cell counts ± SD of a representative experiment from $n = 2$ biological replicates. ****$P \leq 0.0001$ by one-way ANOVA and Dunnett's post hoc test.

Mirali *et al.*, *Sci. Transl. Med.* **12**, eaaz8264 (2020)   8 April 2020

5 of 16

A

B
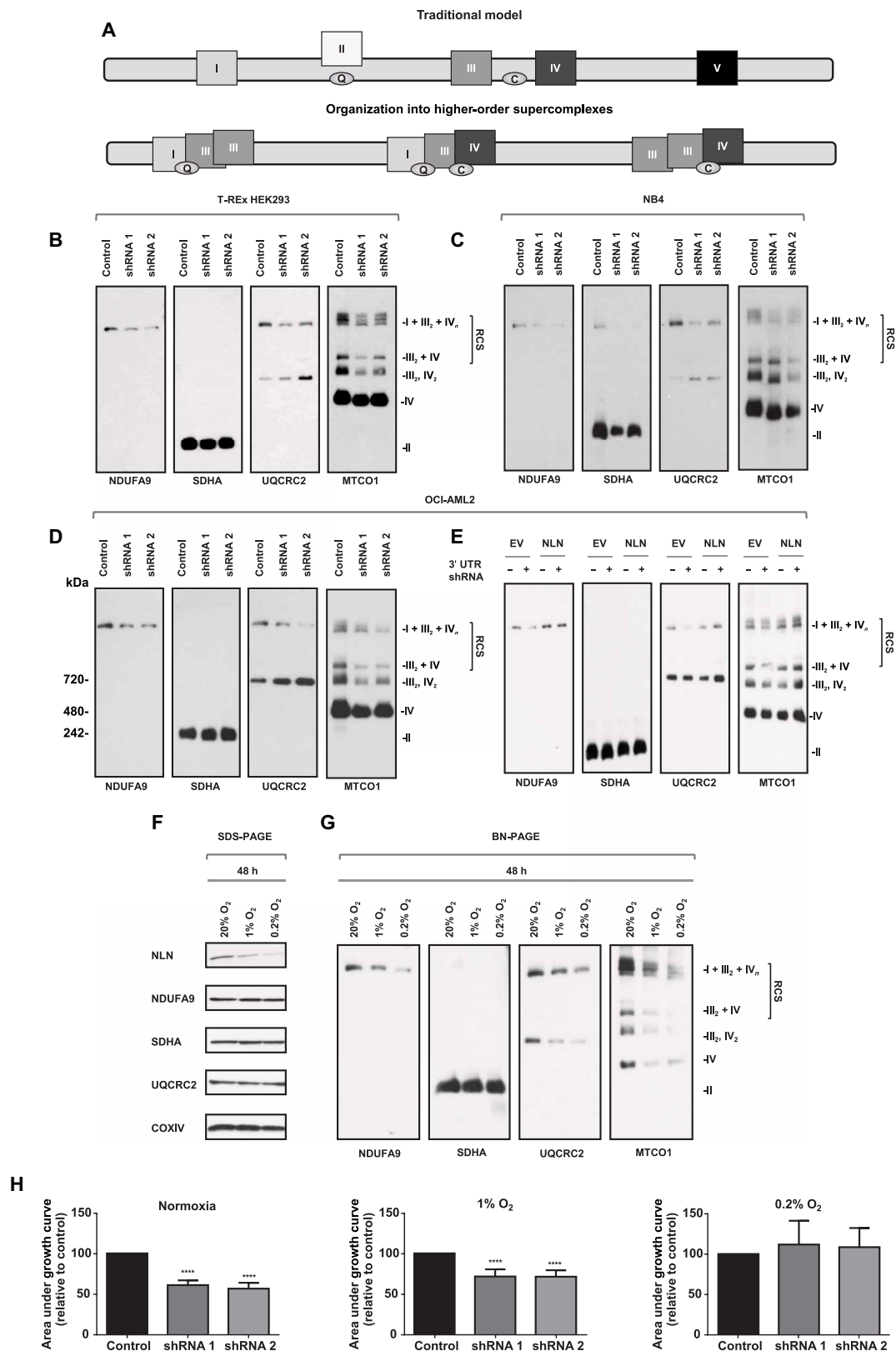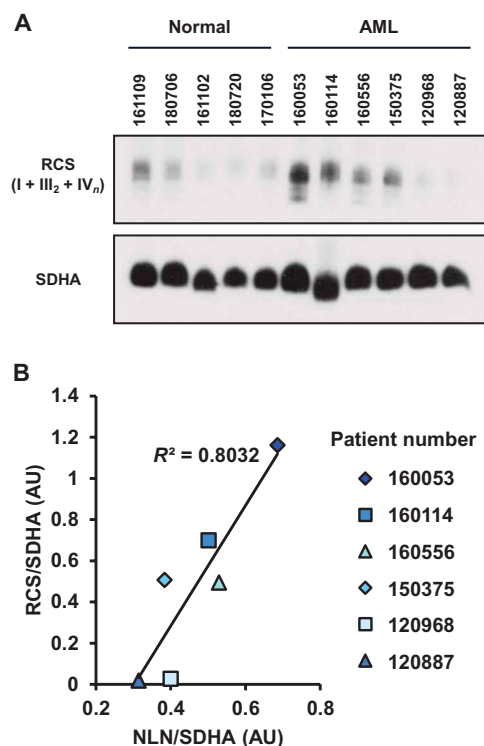
Fig. 4. RCS assembly is enhanced in a subset of patients with AML and correlates with NLN expression. (**A**) Lysates from mitochondria isolated from primary AML and normal hematopoietic cells were analyzed by BN-PAGE with a mixture of antibodies against NDUFA9 (complex I), SDHA (complex II), UQCRC2 (complex III), and MTCO1 (complex IV). (**B**) RCS and NLN in primary AML samples from (A) were semiquantified by densitometry. $R^2 = 0.8032$, $P < 0.05$. AU, arbitrary units.

fraction of 8227 cells (fig. S11D) (23). R2 also decreased the clonogenic growth of primary AML cells (fig. S11E).

To determine whether inhibiting NLN has antileukemia activity in vivo, we assessed the efficacy and toxicity of R2 in an OCI-AML2 xenograft mouse model. Daily treatment with R2 reduced the growth of OCI-AML2 cells in immunodeficient mice (Fig. 6H and fig. S11F) without affecting body weight or causing toxicity (fig. S12, A to G).

Last, we assessed the effects of inhibiting NLN on primary AML and normal hematopoietic cells in vivo. Primary AML and normal hematopoietic cells were injected into the femurs of immunodeficient mice. Two weeks later, mice were treated with R2 or vehicle control. Treatment of mice with R2 reduced the leukemic burden in these mice without toxicity (Fig. 6, I and J, and fig. S12H). Moreover, inhibiting NLN targeted the AML stem cells, as evidenced by decreased engraftment in secondary experiments (Fig. 6K). In contrast, inhibiting NLN did not reduce the engraftment of normal hematopoietic cells (Fig. 6L). Collectively, these results demonstrate that pharmacological inhibition of NLN impairs leukemic cell growth in vitro and in vivo.

DISCUSSION

The function of the mitochondrial peptidase NLN is largely unknown. We showed that NLN maintains efficient oxidative phosphorylation by promoting the formation of RCS. Inhibiting NLN impaired oxidative phosphorylation and targeted AML cells and stem cells in vitro

and in vivo. Thus, this work describes the importance of NLN and RCS in AML and highlights a biological vulnerability in this disease.

NLN is a zinc metallopeptidase localized to the mitochondria and secreted into the circulation. NLN cleaves peptides such as neurotensin and bradykinin in the circulation to regulate blood pressure (6–10), but its mitochondrial function is unclear. To better understand NLN's role in the mitochondria, we profiled NLN's mitochondrial interactors using BioID-MS. An earlier study placed NLN in the mitochondrial intermembrane space (24), but more recent reports localize NLN to the mitochondrial matrix (12–14). Our data are consistent with these more recent reports, as almost all of NLN's mitochondrial interactors are located in the matrix.

NLN interacted with the mitochondrial respiratory chain, and we showed that NLN is necessary for the formation of respiratory chain complexes and supercomplexes. The mitochondrial respiratory chain comprises a series of protein complexes embedded in the inner mitochondrial membrane. The structural organization of the respiratory chain has traditionally been explained by the "fluid state" or "random collision" model. In this model, each complex is an independent entity, and electron transfer depends on the random and transient encounters between the complexes and electron carriers (25). However, recent studies using blue native polyacrylamide gel electrophoresis (BN-PAGE) (26) and cryo–electron microscopy (27) support the "solid state" model, in which respiratory complexes are assembled into large quaternary structures called RCS. RCS consist of complexes I, III, and IV assembled into distinct stoichiometries, such as $I + III_2 + IV_n$ and $III_2 + IV$. The $I + III_2 + IV_n$ supercomplex is also referred to as the "respirasome" because of its ability to directly transfer electrons from NADH (reduced nicotinamide adenine dinucleotide) to oxygen. Recently, a third model called the "plasticity" model has been proposed, in which the complexes coexist in both individual and higher-order structures (28).

Although the existence of supercomplexes is now widely accepted, there is debate regarding the functional advantage of RCS (29). Prior studies suggest that RCS may decrease ROS formation or maintain the stability of individual respiratory chain complexes (30–33). We observed no change in the amounts of ROS after decreasing RCS formation. Rather, in AML cells, RCS formation appears to be necessary for optimal oxidative phosphorylation, because disrupting RCS assembly decreased basal and maximal oxygen consumption. Moreover, RCS formation was decreased under near anoxic conditions, where the cell would have less reliance on oxidative phosphorylation. Thus, RCS are necessary for optimal oxidative phosphorylation in AML. However, RCS may serve different functions in different cell types, which is supported by the fact that the ratio of RCS varies between different tissues and physiological states (15, 34–36).

LETM1 is a 70-kDa mitochondrial protein that forms minor and major complexes. LETM1 is necessary for RCS assembly and proper formation of mitochondrial cristae (20, 37). The subunits of the LETM1 complexes have not been fully mapped, but the AAA–adenosine triphosphatase chaperone, BCS1L, is a component of the LETM1 major complex (20). We discovered that NLN interacts with LETM1 and BCS1L and that inhibition of NLN disrupts the formation of LETM1 complexes. We also demonstrated that knockdown of *LETM1* and *BCS1L* impairs AML growth and oxidative metabolism. Further studies will be necessary to characterize the components of LETM1's minor and major complexes and how NLN regulates LETM1 complex formation.
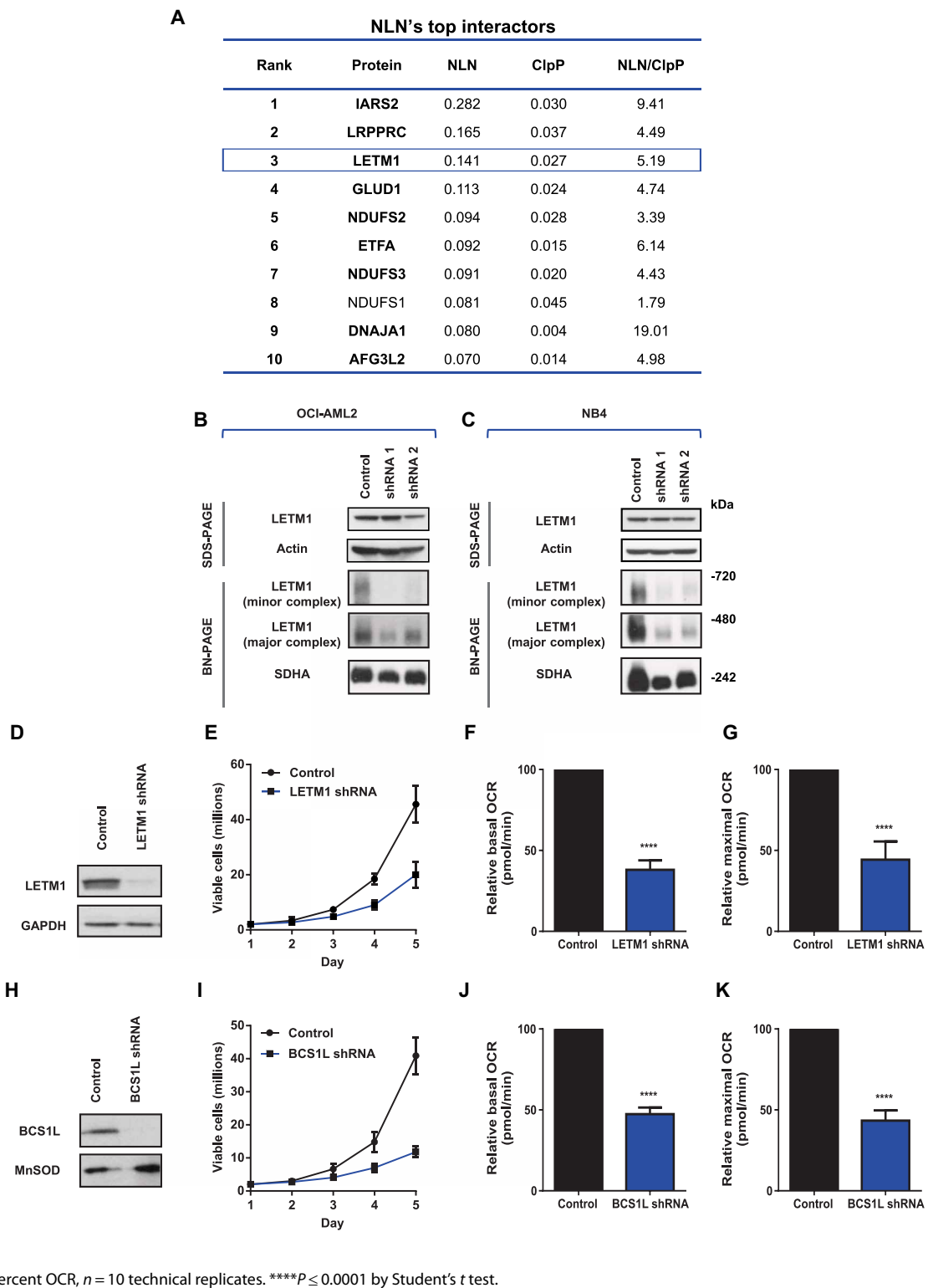
We discovered that inhibiting NLN preferentially targets AML cells and stem cells over normal hematopoietic cells, suggesting a

Mirali *et al.*, *Sci. Transl. Med.* **12**, eaaz8264 (2020)   8 April 2020

6 of 16

Fig. 5. Inhibition of NLN reduces LETM1 complex assembly. (**A**) The top 10 putative mitochondrial protein interactors with NLN identified by BioID-MS compared to their interaction with ClpP. Spectral counts were normalized to each bait's respective BirA* peptide count. Bolded proteins indicate preferential interaction with NLN, defined as >3-fold spectral counts for NLN versus ClpP. (**B** and **C**) Lysates were collected 7 days after OCI-AML2 (B), and NB4 (C) cells were transduced with shRNA targeting *NLN* or control sequences. LETM1 expression was measured by denaturing SDS-PAGE and nondenaturing BN-PAGE gels. LETM1 and SDHA were run in parallel in BN-PAGE. Representative immunoblots of $n = 2$ to 3 biological replicates. (**D**) LETM1 expression in OCI-AML2 cells was measured by immunoblotting 8 days after transducing cells with shRNA targeting *LETM1* or a control sequence. (**E**) Viable cell counts of OCI-AML2 cells seeded 4 days after transducing cells with shRNA targeting *LETM1* or a control sequence. Data points represent mean viable cell counts ± SD of a representative experiment from $n = 2$ biological replicates. (**F** and **G**) Basal (F) and maximal (G) OCR after *LETM1* knockdown in OCI-AML2 cells. Data represent means ± SD percent OCR, $n = 10$ technical replicates. ****$P \leq 0.0001$ by Student's *t* test. (**H**) BCS1L expression in OCI-AML2 cells was measured by immunoblotting 8 days after transducing cells with shRNA targeting *BCS1L* or a control sequence. (**I**) Viable cell counts of OCI-AML2 cells seeded 4 days after transducing cells with shRNA targeting *BCS1L* or a control sequence. Data points represent mean viable cell counts ± SD of a representative experiment from $N = 2$ biological replicates. (**J** and **K**) Basal (J) and maximal (K) OCR after *BCS1L* knockdown in OCI-AML2 cells. Data represent means ± SD percent OCR, $n = 10$ technical replicates. ****$P \leq 0.0001$ by Student's *t* test.

A

NLN's top interactors

| Rank	Protein	NLN	ClpP	NLN/ClpP
1	**IARS2**	0.282	0.030	9.41
2	**LRPPRC**	0.165	0.037	4.49
3	**LETM1**	0.141	0.027	5.19
4	**GLUD1**	0.113	0.024	4.74
5	**NDUFS2**	0.094	0.028	3.39
6	**ETFA**	0.092	0.015	6.14
7	**NDUFS3**	0.091	0.020	4.43
8	NDUFS1	0.081	0.045	1.79
9	**DNAJA1**	0.080	0.004	19.01
10	**AFG3L2**	0.070	0.014	4.98

potential therapeutic window for NLN inhibitors in AML. A potentially favorable toxicity profile for NLN inhibitors is supported by studies of *NLN* KO mice. *NLN* KO mice are viable and are born after following normal Mendelian distribution. They are similar to wild-type mice in external appearance and are fertile. Although NLN degrades several vasoactive peptides, such as neurotensin and bradykinin (*6–10*), *NLN* KO mice have normal blood pressure, indicating that NLN's function in the circulation is redundant (*11*).

Mirali *et al.*, *Sci. Transl. Med.* **12**, eaaz8264 (2020)   8 April 2020

7 of 16

Fig. 6. A small-molecule inhibitor of NLN reduces the growth of leukemic cells and impairs RCS formation. (**A** to **C**) OCI-AML2 (A), NB4 (B), and 8227 (C) cells were treated with R2 (11, 8.6, and 35 μM, respectively) for 72 hours. Mitochondria were isolated, and respiratory chain complexes were measured by immunoblotting denaturing SDS-PAGE and nondenaturing BN-PAGE gels. (**D**) Primary AML patient sample 160053 was treated with 15 μM R2 for 96 hours. Isolated mitochondria were solubilized with digitonin, and RCS formation was measured by BN-PAGE using a mixture of antibodies against NDUFA9 (complex I), SDHA (complex II), UQCRC2 (complex III), and MTCO1 (complex IV). (**E**) OCI-AML2, NB4, and 8227 cells were treated with R2 (11, 8.6, and 25 μM, respectively) for 72 hours. After treatment, LETM1 expression was measured by immunoblotting denaturing SDS-PAGE and nondenaturing BN-PAGE gels. LETM1 and SDHA were run in parallel in BN-PAGE. Representative immunoblots of $N = 2$ to 3 biological replicates. (**F** and **G**) Basal and maximal oxygen consumption rates (OCRs) were measured 72 hours after treatment of OCI-AML2 (F) and 8227 (G) cells with 5 and 25 μM of R2, respectively. Data represent mean percent ± SD OCR, $n = 10$ to 15 technical replicates. ****$P \leq 0.0001$ by Student's t test. FCCP, carbonyl cyanide p-trifluoromethoxyphenylhydrazone. (**H**) Immunodeficient mice with OCI-AML2 xenografts were treated with R2 (100 mg/kg) or vehicle control daily five times per week for 2 weeks. Tumor volume was measured over time ($n = 10$ mice per group). Data represent means ± SD. *$P \leq 0.05$, ****$P \leq 0.0001$ by two-way ANOVA and Bonferroni's post hoc test. (**I** and **J**) Primary AML cells from patient 120541 (I) and 120287 (J) were injected into the femurs of sublethally irradiated female immunodeficient mice. Ten days after injection, mice were treated with R2 (100 mg/kg by intraperitoneal injection) or vehicle control three times per week. Four weeks

after treatment, mice were euthanized and the number of human CD45$^+$CD33$^+$CD19$^-$ cells in the noninjected femur was measured by flow cytometry. Horizontal bar represents mean engraftment of human cells ($n = 8$ to 10 mice in control group, $n = 9$ to 10 mice in R2 group). ****$P \leq 0.0001$ by Student's t test. (**K**) Secondary engraftment of cells from AML patient 120541 was assessed by injecting equal numbers of viable leukemia cells from the bone marrow of R2-treated and vehicle mice into the right femur of untreated irradiated female immunodeficient mice. Six weeks after injection, mice were euthanized and the number of human CD45$^+$CD33$^+$CD19$^-$ cells in the noninjected femur was measured by flow cytometry. Horizontal bar represents mean engraftment of human cells ($n = 6$ mice in control group, $n = 5$ mice in R2 group). *$P \leq 0.05$ by Student's t test. (**L**) Normal human cord blood was injected into the femurs of sublethally irradiated female immunodeficient mice. Ten days after injection, mice were treated with R2 (100 mg/kg by intraperitoneal injection) or vehicle control three times per week. Four weeks after treatment, mice were euthanized and the number of human CD45$^+$CD33$^+$CD19$^-$ cells in the noninjected femur was measured by flow cytometry. Horizontal bar represents mean engraftment of human cells ($n = 4$ mice in control group, $n = 5$ mice in R2 group). $P > 0.05$ by Student's t test. NS, not significant.

Mirali *et al.*, *Sci. Transl. Med.* **12**, eaaz8264 (2020)   8 April 2020

8 of 16
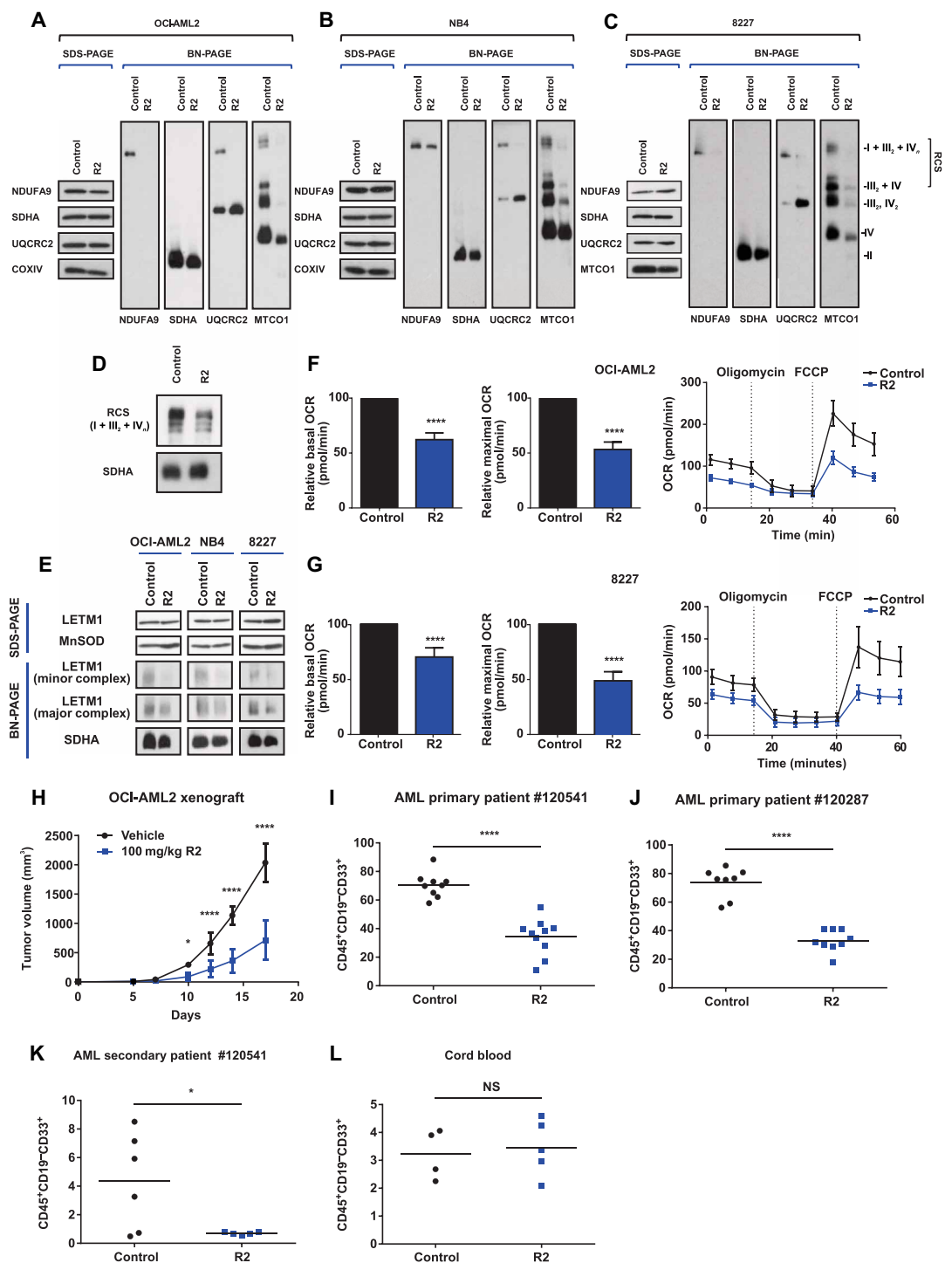
Consistent with our findings that NLN is necessary for RCS formation, *NLN* KO mice demonstrate mild metabolic defects. KO mice have greater insulin sensitivity, increased glucose tolerance, and increased liver gluconeogenesis. Moreover, muscle from KO mice show fewer oxidative fibers, and KO mice perform worse on measures of exercise endurance (*11*).

Our study has a number of limitations. Because NLN is present in the central nervous system, pharmacological inhibition of NLN may affect nociception and dopaminergic pathways (*6*, *10*). These side effects may be mitigated by ensuring that the drug does not cross the blood-brain barrier. Moreover, although R2 was initially designed to inhibit NLN, it may also inhibit the closely related cytosolic peptidase, THOP1. Thus, we cannot exclude the possibility that some of R2's effects may be due to THOP1 inhibition, and future work will be needed to study the relative contributions of THOP1 and NLN inhibition to impairment of leukemic growth. Although R2 may inhibit both peptidases, we found that *NLN* knockdown does not affect the expression of THOP1. Last, NLN may be mediating RCS formation dependent or independent of its peptidase activity. NLN has previously been shown to degrade mitochondrial presequence peptides (*14*). Future studies will need to investigate whether NLN is processing LETM1 or respiratory chain complex subunits upon their import into the mitochondria and whether this function is dependent or independent of NLN's peptidase activity. Moreover, although *NLN* knockdown does not affect the expression of OPA1, it is possible that RCS assembly is secondary to malformation of cristae. Further studies should focus on refining this aspect of NLN's mechanism.

The preferential effects of NLN on AML cells over normal hematopoietic cells are in line with previous reports that AML cells and stem cells have increased flux of substrates into the tricarboxylic acid cycle and decreased spare reserve capacity in their respiratory chain (*3*, *4*, *38*). Hence, hampering oxidative phosphorylation in AML by disrupting RCS formation with NLN inhibitors could selectively target AML cells.

In conclusion, we report that NLN is necessary for RCS formation, and RCS are necessary for oxidative metabolism in AML. Thus, RCS formation represents a biological vulnerability in AML cells. Moreover, we highlight inhibition of NLN as a therapeutic strategy for AML.

MATERIALS AND METHODS
Study design
The purpose of this study was to determine NLN's mitochondrial function and to investigate its role in AML. *NLN* expression in AML and normal bone marrow was determined by analysis of publicly available gene expression datasets and immunoblotting. NLN's function was assessed by genetic (shRNA) and chemical inhibition of NLN in vitro and in vivo. To identify NLN's protein interactors, we used BioID-MS. For in vivo studies, mice were randomly assigned to treatment arms. For patient-derived xenograft mouse models, the primary end point was leukemia burden in the bone marrow at study completion. Treatment assignment was not blinded. Sample size was calculated on the basis of previous work where 10 mice per group were needed to achieve statistical significance. Treatment duration was established before starting each experiment. All available data points were included in the analysis.

Bioinformatic analysis
Affymetrix gene expression data of AML (536 samples) and healthy bone marrow samples (73 samples) from the Haferlach dataset (*39*)

were downloaded from the Leukemia Gene Atlas portal in March 2016. The platform used was Affymetrix Human Genome U133 Plus 2.0 Array, and the data values correspond to robust multichip average expression measures. Official gene symbols from the HUGO Gene Nomenclature Committee were retrieved from the Affymetrix probe identifiers using the R package biomaRt (biomaRt_2.26.1 and R version 3.2.3) and searched against Ensembl Genes version 84. Data were reduced at the gene level by selecting the probe with the highest median absolute deviation across samples per gene.

To study the gene expression patterns within the AML samples and make comparisons between patients with AML and normal controls, data were centered, scaled (*z* score), and clustered using the heatmap.2 function available from the gplots R package (gplots_2.17.0). For each pair of samples, the Euclidean distance based on NLN expression values was calculated to create the distance matrix. Hierarchical clustering using the complete linkage method was applied to identify the main groups of samples that showed a minimum distance between them, and the result was visualized using a dendrogram. The samples and associated gene expression values for the four main AML clusters were retrieved from the hierarchical cluster results using the cutree function in R. A boxplot was constructed using the *z* score values for the four AML groups and the group of normal samples. Overexpression was defined as 1 SD above the mean NLN expression of normal bone marrow.

One-way analysis of variance (ANOVA) and pairwise *t* tests were applied to the data to test the significance of the differences in the mean values between the groups. Using the default parameters, each row (gene) in the result has a mean of 0 and a sample SD of 1. The *z* score is a normalized value, indicating how many SDs away the gene expression is compared with the mean expression of all samples for the same gene: $z = (x - \mu)/\sigma$, where x is the gene expression, μ is the mean gene expression across samples, and σ is the SD of the population.

To assess NLN expression in CD34$^+$/CD34$^-$ and LSC$^+$/LSC$^-$ AML fractions, normalized Illumina BeadChip transcriptomics data containing LSC$^+$/LSC$^-$ and CD34$^+$/CD34-sorted AML fractions were obtained from the Gene Expression Omnibus data portal (GSE76008) (*18*). Boxplots were constructed using the NLN expression of the samples divided into four categories: LSC$^+$, LSC$^-$, CD34$^+$, and CD34$^-$.

To measure the degree of correlation between *NLN* expression and AML mutations, Beat AML data were downloaded from supplementary tables in the paper "Functional genomic landscape of acute myeloid leukaemia" (*40*). The counts per million table, table S9 from (*40*), consists of 22,843 genes and 451 patients. The clinical table, table S5 from (*40*), includes 672 tumor specimens collected from 562 patients. We tested the degree of correlation between *NLN* expression and AML mutations using three methods: (i) *t* test and (ii) Wilcoxon rank sum test between mutated and nonmutated patients: The *t* test and Wilcoxon rank sum test were to compare *NLN* gene expressions between two groups of patients with or without AML mutations. (iii) The Fisher's exact test evaluates the significance of the overlap size between two groups of patients with NLN defined by low or high *NLN* expression (greater or lesser than the median) and the two groups of mutated and nonmutated patients. The null hypothesis is the independence of the *NLN* expression category (high or low) and the mutation status (0 or 1).

Cell lines
Flp-In T-REx HEK293 cells (Thermo Fisher Scientific R71007) were grown in Dulbecco's modified Eagle's medium (DMEM) containing

Mirali *et al.*, *Sci. Transl. Med.* **12**, eaaz8264 (2020)   8 April 2020

9 of 16

penicillin (100 U/ml) and streptomycin (100 µg/ml; Wisent) and supplemented with 10% fetal bovine serum (FBS) (Sigma). OCI-AML2 (provided by M. D. Minden) and MV4-11 cells [American Type Culture Collection (ATCC) CRL-9591] were grown in Iscove's modified Dulbecco's medium (IMDM) containing penicillin (100 U/ml) and streptomycin (100 µg/ml; Wisent) and supplemented with 10% FBS. NB4 cells [Deutsche Sammlung von Mikroorganismen und Zellkulturen (DSMZ) ACC-207] were grown in RPMI 1640 medium containing penicillin (100 U/ml) and streptomycin (100 µg/ml; Wisent) and supplemented with 10% FBS. TEX leukemia cells obtained from J. Dick's lab (19) were maintained in IMDM with 20% FBS, 2 mM L-glutamine (Thermo Fisher Scientific 25030081), human recombinant stem cell factor (20 ng/ml) (SCF) (R&D Systems 255-sc), and human recombinant interleukin-3 (2 ng/ml; IL-3) (R&D Systems 203-IL). A total of 8227 cells were obtained from J. Dick's lab (23) and were cultured in X-VIVO 10 (Lonza 04-380Q) with 20% bovine serum albumin (BSA)–insulin-transferrin (STEMCELL Technologies 09500), human Fms-related tyrosine kinase 3 ligand (Flt3-L; 50 ng/ml) (PeproTech 300-19), IL-6 (10 ng/ml) (PeproTech 200-06), SCF (50 ng/ml) (PeproTech 300-07), thrombopoietin (25 ng/ml) (PeproTech 300-18), IL-3 (10 ng/ml) (PeproTech 200-03), and granulocyte colony-stimulating factor (G-CSF; 10 ng/ml) (Amgen 121181-53-1). Lentiviral packing cells (293T) (ATCC CRL-11268) were cultured in DMEM with 10% FBS for seeding and DMEM with 10% FBS, penicillin (100 U/ml), streptomycin (100 µg/ml), and 1% BSA for harvesting of virus. All cell lines were maintained at 37°C, supplemented with 5% CO_2 in a humidified atmosphere. The sex and age of the patients from whom the cell lines were generated are indicated in table S2.

Primary AML and normal hematopoietic cells
Primary human AML samples were obtained from peripheral blood or the bone marrow of consenting male or female patients with AML, with a malignant cell frequency of 80% among mononuclear cells. Differential density centrifugation was used to isolate AML cells. Peripheral blood stem cells (PBSCs) were obtained from healthy consenting male or female volunteers donating PBSCs for allogenic stem cell transplantation. PBSCs were isolated by G-CSF stimulation and leukapheresis. Primary AML cells and PBSCs were frozen in alpha MEM + 5% FBS or 90% FBS + heparin (15 U/ml) + 10% dimethyl sulfoxide (DMSO). The University Health Network institutional review board approved the collection and use of human tissue for this study (Research Ethics Board protocol no. 13-7163). All specimens were deidentified, and each experiment was performed using a single aliquot from a donor. Information about the patients who were the source of the cells is provided in table S3.

Animals
Eight- to 12-week-old male or female immunodeficient NOD.Cg-Prkdc^scid IL2rg^tm1Wjl Tg (CMV-IL3,CSF2,KITLG)1Eav/MloySzJ [NOD–severe combined immunodeficient (SCID)–growth factor (GF)] mice used to transplant TEX and 8227 cells were obtained from C. J. Eaves and bred in our facility (41). Eight- to 12-week-old female immunodeficient NOD.CB17-Prkdc^scid/J (NOD-SCID) and 6- to 8-week-old immunodeficient male Prkdc^scid (SCID) mice, used for the transplantation of primary AML and OCI-AML2 cells, respectively, were obtained from the University Health Network. Mice were randomly assigned to each experimental group.

During all experiments, the weights of the mice were about 18 to 30 g, with no animals losing greater than 10% body weight. All animals were housed in microisolator cages with temperature-controlled conditions under a 12-hour light/dark cycle with access to drinking water and food. Only one experimental procedure was performed on each mouse, and all mice were drug naïve before the experiment. All animal studies were performed in accordance with the University Health Network Animal Use Protocol no. 1251.34 (NOD-SCID-GF, NOD-SCID, and SCID).

Viral infections
The hairpin-pLKO.1 vectors (carrying the puromycin antibiotic resistance gene) containing the shRNA sequences used are as described previously (1). The hairpin-pLKO.1 vector was isolated using the E.N.Z.A. Plasmid Midi Kit system (Omega Bio-tek) and then quantified with a NanoDrop (Thermo Fisher Scientific) spectrophotometer. Lentiviruses were made in a 25-cm² flask, by transfecting HEK293T cells with a three-plasmid system (hairpin-pLKO.1 vector, packaging plasmid with *gag*, *pol*, and *rev* genes and envelope plasmid). All plasmids were validated by Sanger sequencing before use.

The coding sequences of shRNAs targeting *NLN* (accession no. NM_020726) are as follows: shRNA1, 5′-CCGGGCATGGACAT-GCTCCACAATTCTCGAGAATTGTGGAGCATGTCCAT-GCTTTTTG-3′; shRNA 2, 5′-CCGGGCAGATGTAGAAGTAAAG-TATCTCGAGATACTTTACTTCTACATCTGCTTTTTG-3′; 3′ untranslated region (UTR) shRNA, 5′-CCGGTGGAGCTCTGT-GTCAACTTTGCTCGAGCAAAGTTGACACAGAGCTC-CATTTTTG-3′. The coding sequence of shRNA targeting LETM1 (accession no. NM_012318) is as follows: shRNA, 5′- CCGGGC-TATGGATCGACACCAAGATCTCGAGATCTTGGTGTC-GATCCATAGCTTTTTG-3′. The coding sequence of shRNA targeting BCS1L (accession no. NM_004328) is as follows: shRNA, 5′- CCG-GGCTGAGAACTTTGCAGAACATCTCGAGATGTTCTG-CAAAGTTCTCAGCTTTTT-3′.

shRNA knockdown in AML cell lines
To perform lentiviral transductions, we resuspended 5×10^6 OCI-AML2, NB4, and TEX cells or 2×10^5 Flp-In T-REx HEK293 cells in 5 ml of medium containing protamine sulfate (5 µg/ml; MP Biomedicals 194729). Two milliliters of virus was added to OCI-AML2 and TEX cells, 1 ml to NB4 cells, or 300 µl to Flp-In T-REx HEK293 cells, followed by an overnight incubation (37°C, 5% CO_2). The following day, fresh medium with puromycin (1.5 µg/ml for OCI-AML2, T-REx HEK293, and NB4 or 2 µg/ml for TEX) was added to cells. Three days later, the medium was replaced with nonpuromycin-containing medium.

To perform lentiviral transductions on MV4-11 cells, 12-well nontissue culture–treated plates were coated with RetroNectin, blocked with 2% BSA, and stored at 4°C overnight. The next day, the BSA was aspirated, 2 ml of virus was added to each well, and the plates were centrifuged at 3000 revolutions per minute (rpm) for 2.5 hours. The viral supernatant was aspirated, and 1×10^6 MV4-11 cells in 1 ml of medium was added to each well. Two days later, fresh medium with puromycin (0.5 µg/ml) was added to cells. Three days later, the medium was replaced with nonpuromycin-containing medium.

NLN overexpression
For experiments overexpressing *NLN*, the human *NLN* open reading frame (ORF) clone (OriGene, no. RC212447) was subcloned into the pLentiEF1α vector (carrying the blasticidin antibiotic resistance gene), and a STOP codon was added at the end of the ORF so that the vector would express *NLN* without a tag (pLentiEF1α-hNLN).

Mirali *et al.*, *Sci. Transl. Med.* **12**, eaaz8264 (2020) 8 April 2020

10 of 16

The empty vector, pLentiEF1α, served as a control. OCI-AML2 cells were seeded in T25 flasks at 5×10^5 cells/ml (3 ml per flask). The culture was supplemented with protamine sulfate (1 μg/ml). To each flask, we added 1 ml of either pLentiEF1α or pLentiEF1α-*NLN* viral stock, followed by overnight incubation (37°C, 5% CO_2). The following day, 1 ml of virus containing shRNA targeting a control sequence (*GFP*) or the 3′ UTR of *NLN* was added and incubated overnight. The next day, cells were resuspended in 20 ml of medium containing both blasticidin (10 μg/ml) and puromycin (1.5 μg/ml), incubated for 3 days, and then subcultured at a concentration of 1:20 in 20 ml of fresh medium containing blasticidin (10 μg/ml) and puromycin (1.5 μg/ml) for 3 days. Cells were then subcultured at a concentration of 2×10^4 cells/ml in fresh medium with blasticidin (10 μg/ml) for 5 days. Cells were collected for immunoblot lysate and seeded at a concentration of 1×10^5 cells/ml in fresh medium and counted over 4 days.

Mitochondrial protein lysates
To isolate mitochondria from cell lines and primary patient samples, 1 to 4×10^7 cells were washed in phosphate-buffered saline (pH 7.4), resuspended in 500 μl mitochondrial isolation buffer [200 mM sucrose, 10 mM tris/Mops (pH 7.2), and 1 mM EGTA/tris] with protease inhibitors (Thermo Fisher Scientific 87786) and transferred to a glass dounce homogenizer. Cells were homogenized until 5 to 10% of cells were viable as assessed by trypan blue exclusion staining. The lysate was then centrifuged at $600g$ for 10 min at 4°C. The supernatant was removed and centrifuged at $7000g$ for 10 min at 4°C. The supernatant was discarded, and the pellet was resuspended in cold mitochondrial isolation buffer with protease inhibitors. Protein concentration was quantified using the Pierce BCA Protein Assay Kit (Thermo Fisher Scientific 23225).

Immunoblotting
Mitochondrial isolates or total cell lysates from cell lines or primary patient samples were lysed using radioimmunoprecipitation assay buffer, and mitochondrial protein concentration was measured by the Bradford assay (Bio-Rad). Equal amounts of protein were run on 10 to 12% SDS-PAGE gels and transferred to polyvinylidene difluoride (PVDF) membranes. Membranes were blocked with 5% milk in Tris-buffered saline with Tween 20 (TBST) for 1 hour and then incubated with primary antibody dissolved in 5% milk in TBST overnight at 4°C. Primary antibodies included anti–glyceraldehyde-3-phosphate dehydrogenase (GAPDH) (Cell Signaling Technology CST-2118S), anti-tubulin (Cell Signaling Technology CST 2144), anti-actin (Santa Cruz Biotechnology sc-69879), anti-NLN (Abcam ab119802), anti-THOP1 (Thermo Fisher Scientific PA5-48031), anti-LETM1 (Abcam 55434), anti-NDUFA9 (Abcam ab14713), anti-NDUFB8 (Abcam ab110242), anti-succinate dehydrogenase complex flavoprotein subunit A (SDHA) (Abcam ab14715), anti-UQCRC2 (Abcam ab14745), anti-MTCO1 (Abcam ab14705), anti-COXIV (Thermo Fisher Scientific A-21347), anti-ATP5B (Abcam ab14730), anti-MnSOD (Enzo ADI-SOD-110), and anti-BCS1L (Abnova H00000617-M01). The membranes were washed three times before incubation for 1 hour at room temperature with secondary horseradish peroxidase–conjugated donkey anti-rabbit antibody (GE Healthcare), sheep anti-mouse antibody (GE Healthcare), or donkey anti-sheep antibody (Thermo Fisher Scientific).

Cell growth and viability assays
Three days after shRNA knockdown of target genes, equal numbers of cells were plated to assay growth. Cells were counted by trypan

blue exclusion staining for a period of 8 days after transduction. To confirm target knockdown, 5 to 20×10^6 cells were collected at day 7 after transduction for immunoblot analysis.

R2 was obtained from Dalriada and J&C consulting with purity over 90%. For R2 dose response curves, cells were plated in 96-well plates at 10,000 cells in 100 μl of medium per well. After 3 days of treatment, 100 μl of CellTiter-Fluor (Promega) was added to each well. Plates were incubated at 37°C for 2 to 3 hours before measuring fluorescence with SpectraMax M3 plate reader at an excitation of 380 to 400 nm and an emission of 505 nm. Background fluorescence value of medium-only wells was subtracted from each reading. Viability was determined after normalization to vehicle control treatment.

Colony formation assays
Seven days after transduction of OCI-AML2 and NB4 cells with control shRNA or one of two different shRNA sequences targeting *NLN*, 750 cells were plated in duplicate 35-mm dishes (Nunclon) to a final volume of 1 ml per dish in MethoCult H4100 medium (STEMCELL Technologies) supplemented with 30% FBS. After incubating the dishes for 10 days at 37°C, 5% CO_2 with 95% humidity, the number of colonies containing 10 or more cells was counted on an inverted microscope. The mean of the duplicate plates for each condition is presented.

To assess clonogenic growth in primary samples, 4×10^5 fresh AML mononuclear cells were incubated with R2 or vehicle control for 72 hours in Myelocult H5100 (STEMCELL Technologies), supplemented with rhSCF (100 ng/ml), rhFlt3-L (10 ng/ml), rhIL-7 (20 ng/ml), rhIL-3 (10 ng/ml), rhIL-6 (20 ng/ml), rhG-CSF (20 ng/ml), and rhGM-CSF (20 ng/ml). Treated AML patient samples were plated in MethoCult H4434 medium (STEMCELL Technologies). After incubating the dishes for 7 days at 37°C with 5% CO_2 and 95% humidity, AML colonies containing 10 or more cells were counted. The mean of duplicate plates for each condition are presented.

TEX engraftment
Equal numbers of TEX cells (2×10^5) transduced with shRNA in lentiviral vectors targeting *NLN* or a control sequence were injected into the right femur of sublethally irradiated NOD-SCID-GF mice expressing human IL-3, GM-CSF, and steel factor (*41*). Five weeks after injection, mice were euthanized, and the percentage of human CD45$^+$ (BD Biosciences) was enumerated in TEX cells by flow cytometry.

Proximity-dependent biotinylation
BioID-MS was conducted as described previously (*42*). *NLN* or *ClpP* complementary DNA (cDNA) was fused in-frame with a mutant *Escherichia coli* biotin-conjugating enzyme, BirA R118G (or BirA*) into a tetracycline-inducible pcDNA5 FLP recombinase target/ tetracycline operator (FRT/TO) expression vector, which was then transfected into Flp-In T-REx HEK293 Flp-In cells. Cells were lysed, sonicated twice for 10 s at 35% amplitude (Sonic Dismembrator 500; Fisher Scientific), and centrifuged at $35,000g$ for 30 min at 4°C. Supernatants were passed through a Micro Bio-Spin chromatography column (Bio-Rad 732-6204) and incubated with 30 μl of high-performance streptavidin packed beads (GE Healthcare) for 3 hours at 4°C on an end-over-end rotator. Beads were collected (2000 rpm, 2 min) and washed six times with 50 mM ammonium bicarbonate (pH 8.3). Beads were then treated with L-1-tosylamide-2-phenylethyl chloromethyl ketone (TPCK)–trypsin (Promega) for 16 hours at 37°C on an end-over-end rotator. After 16 hours, another

Mirali *et al.*, *Sci. Transl. Med.* **12**, eaaz8264 (2020)   8 April 2020

11 of 16

1 µl of TPCK-trypsin was added for 2 hours and incubated in a water bath at 37°C. Supernatants were lyophilized and stored at 4°C for downstream MS analysis. Two biological and two technical replicates were completed for each protease. NLN's interactors were compared to ClpP's interactors, which were normalized to each protease's respective BirA* spectral counts.

Liquid chromatography–MS

Liquid chromatography was conducted using a C18 precolumn (inner diameter, 2 cm × 75 µm; Acclaim PepMap 100; Thermo Fisher Scientific) and a C18 analytical column (inner diameter, 50 cm × 75 µm; Acclaim PepMap rapid separation liquid chromatography (RSLC); Thermo Fisher Scientific), running a 120-min reversed-phase gradient (0 to 40% acetonitrile (ACN) in 0.1% formic acid) at 225 nl/min on an EASY-nLC1200 pump (Proxeon) in-line with a Q Exactive HF mass spectrometer (Thermo Fisher Scientific). An MS scan was performed with a resolution of 60,000 (full width at half maximum), followed by up to 20 tandem MS (MS/MS) scans (minimum ion count of 1000 for activation) using higher-energy collision-induced dissociation fragmentation. Dynamic exclusion was set for 5 s [10 parts per million (ppm); exclusion list size = 500].

MS data analysis

For peptide and protein identification, Thermo .RAW files were converted to the .mzML format using ProteoWizard (v3.0.10800) (43) and then searched using X! Tandem [X! TANDEM Jackhammer TPP (v2013.06.15.1)] (44) and Comet (v2014.02 rev.2) (45) against the human Human RefSeq v45 database (containing 36113 entries). Search parameters specified a parent ion mass tolerance of 10 ppm and an MS/MS fragment ion tolerance of 0.4 Da, with up to two missed cleavages allowed for trypsin [excluding lysine/arginine proline (K/RP)]. Variable modifications included deamidation on N and Q, oxidation on M, GG on K, and acetylation on protein N terminus in the search. Data were filtered through the trans-proteomic pipeline (TPP) (v4.7 POLAR VORTEX rev 1) with general parameters set as –p0.05 -x20 –PPM.

Proteins were identified with an iProphet cutoff of 0.9, and at least two unique peptides were analyzed with significance analysis of interactome (SAINT) Express (v.3.6) (46, 47). Control runs (21 runs from cells expressing the FlagBirA* epitope tag only) were collapsed to the two highest spectral counts for each prey, and high-confidence interactors were defined as those with an Bayesian false discovery rate (BFDR) of ≤0.01. ProHits-viz was used for bait-bait Pearson Correlations and heat map generation. All raw MS files have been deposited at the MassIVE archive (massive.ucsd.edu), ID MSV000084182.

Seahorse assays

OCR was measured in AML cells after shRNA knockdown or drug treatment using the Seahorse XF Cell Energy Phenotype Test Kit (Agilent, 103325-100) following manufacturer's protocol. Data were collected using the Seahorse XF-96 analyzer (Seahorse Bioscience). Seven days after transduction or 3 days after treatment with R2, cells were resuspended in unbuffered XF assay medium (Agilent, 102365-100) supplemented with 2.5 mM glucose and 1 mM sodium pyruvate and seeded at 1.2×10^5 cells per well in Cell-Tak–coated (0.15 µg per well) XF96 plates. Cells were equilibrated in the unbuffered XF assay medium for 1 hour at 37°C in a CO_2-free incubator before being transferred to the XF96 analyzer.

Electron microscopy

OCI-AML2 cells were transduced with shRNA targeting NLN or control sequences in lentiviral vectors. Seven days after transduction, cells were harvested and imaged by transmission electron microscopy. Briefly, cells were harvested and fixed in a Graham-Karnovsky's style fixative [4% paraformaldehyde and 2% glutaraldehyde in 0.1 M phosphate buffer (pH 7.2)] for 1 hour at room temperature. Cells were postfixed with 1% osmium tetroxide, dehydrated with ethanol, washed with propylene oxide, treated with epoxy resin polymerized at 60°C for 48 hours, sectioned on a Reichert Ultracut E microtome to a thickness of 90 nm, collected on 300-mesh copper grids, and counterstained with uranyl acetate and lead citrate. A Hitachi H-7000 (Hitachi) transmission electron microscope was used to evaluate the sections at an accelerating voltage of 75 kV.

Mitochondrial membrane potential

To measure mitochondrial membrane potential, OCI-AML2 cells were plated in 96-well suspension U-bottom plates and incubated for 15 min with 2.5 µM of 5,5′,6,6′-tetrachloro-1,1′,3,3′-tetraethyl benzimidazolylcarbocyanine iodide (JC-1, Cayman) at 37°C, 5% CO_2 in the dark. After incubation, cells were centrifuged at 1000 rpm for 3 min, the supernatant was removed, and cells were resuspended in 0.2 ml of Annexin V–allophycocyanin (APC) and run on Fortessa HTS flow cytometer using a 561-nm laser (48). Analysis was conducted using FlowJo version 7.7.1 (TreeStar). To obtain the mitochondrial membrane potential (FL2/FL1) for Annexin V–negative cells, emission from the red channel was divided by emission from the green channel.

Mitochondrial mass

To measure mitochondrial mass, OCI-AML2 cells were centrifuged at 1700 rpm for 10 min and stained with 100 nM MitoTracker Deep Red FM (Molecular Probes) in Phenol Red-free Hank's Buffer for 30 min at 37°C in the dark 7 days after transduction. After incubation, cells were centrifuged and stained with Annexin V–fluorescein isothiocyanate (FITC), and flow cytometry was performed in a Fortessa HTS cytometer (BD Biosciences). Data were analyzed with FlowJo version 7.7.1 (TreeStar).

Mitochondrial ROS

To measure mitochondrial ROS, OCI-AML2 cells were suspended in 0.2 ml of 5 µM MitoSOX (Molecular Probes/Life Technologies) and incubated in the dark for 30 min at 37°C and 5% CO_2 in humidified atmosphere 7 days after transduction. Cells were then centrifuged to remove the dye, resuspended in 0.2-ml binding buffer containing Annexin V–FITC (BioVision), and analyzed by flow cytometry on a Fortessa HTS cytometer (BD Biosciences). Antimycin A (50 µM; Sigma) treatment was used as positive control for increased ROS production. The percentages of Annexin V–negative and MitoSOX-positive cells were determined, and the fold increase of ROS production was calculated.

Cellular ROS

To measure cellular ROS, OCI-AML2 cells were suspended in 10 µM carboxy-H_2DCFDA (Molecular Probes/Life Technologies) and incubated in the dark for 30 min at 37°C and 5% CO_2 in humidified atmosphere 7 days after transduction. Cells were then centrifuged to remove the dye, resuspended in 0.2-ml binding buffer containing Annexin V–APC (eBioscience), and analyzed by

flow cytometry on a Fortessa HTS cytometer (BD Biosciences). A total of 0.03% (v/v) of hydrogen peroxide (Sigma) treatment was used as a positive control for increased ROS production. The percentages of Annexin V–negative and carboxy-H$_2$DCFDA–positive cells were determined, and the fold increase of ROS production was calculated.

Blue NativePAGE
For cell lines, mitochondria were harvested 7 days after transduction or 3 days after treatment with R2. For primary patient samples and normal PBSCs, mitochondria were harvested immediately after thawing. Protein lysis and extraction were performed with digitonin (8 g/g) and NativePAGE (Invitrogen) buffer for 20 min on ice. The lysates were cleared by centrifugation at 20,000g for 10 min at 4°C. Lysates were quantified using the Pierce BCA Protein Assay Kit (Thermo Fisher Scientific 23225), and G-250 dye (2 g/g) was added immediately before the samples were loaded on a 3 to 12% Invitrogen NativePAGE gel (BN1003BOX; Invitrogen) and transferred to a PVDF membrane.

Image quantification
Images were scanned and converted to 16-bit with ImageJ. Quantification was performed with the Plot Lanes function. The peaks were selected and quantified from the plots.

Protein purification and crystallization
Human ClpP was expressed and purified as described previously (49–51). Wild-type human ClpP (without mitochondrial targeting sequences) was cloned into pETSUMO2 expression vectors and expressed in *E. coli* SG1146 (50). To induce protein expression, bacteria were treated with 1 mM isopropyl-1-thio-B-D-galactopyranoside for 4 hours at 37°C after reaching an OD$_{600}$ (optical density at 600 nm) of ~0.6, harvested by centrifugation, and disrupted in lysis buffer [25 mM tris-HCl (pH 7.5), 500 mM NaCl, and 10% glycerol], by sonication. After cell lysis, the insoluble material was removed by centrifugation [27,000g (Sorvall rotor SS-34) for 30 min twice], and the supernatant was passed through a 10-ml Ni-sepharose high-performance column (GE Healthcare) pre-equilibrated with lysis buffer. The protein was washed with four wash buffers [25 mM tris-HCl (pH 7.5), 500 mM NaCl, and 10% glycerol] containing 50, 100, 150, and 200 mM imidazole, respectively, and eluted with 25 mM tris-HCl (pH 7.5), 500 mM NaCl, 10% glycerol, and 400 mM imidazole. The protein was diluted with 25 ml of dialysis buffer [50 mM tris-HCl (pH 7.5), 0.3 M NaCl, and 10% glycerol], mixed with SUMO protease (1:100) (52), and dialyzed overnight at 4°C with light stirring into 4 liters of dialysis buffer using Slide-A-Lyzer Dialysis Cassettes 3K (Thermo Fisher Scientific). The dialyzed material was then passed through a second 10-ml Ni-column (Thermo Fisher Scientific), and the flow-through solution containing untagged ClpP was collected. All fractions were analyzed by SDS-PAGE.

Human ClpX was expressed and purified as described previously (1). His-tagged wild-type human ClpX was transformed into BL21 Gold DE3 competent *E. coli* (New England BioLabs). Transformed bacteria were plated on LB agar plates containing ampicillin (100 μg/ml) and incubated overnight at 37°C. The following day, individual colonies were grown overnight at 37°C in LB medium containing ampicillin (100 μg/ml). To induce protein expression, bacteria were treated with 1 mM isopropyl-1-thio-B-D-galactopyranoside for 4 hours at 37°C in Terrific medium containing ampicillin (100 μg/ml) after reaching OD$_{600}$ of ~0.6, harvested by centrifugation, and disrupted in lysis

buffer [30 mM Hepes (pH 8.0), 300 mM NaCl, 10% glycerol, 2 mM mercaptoethanol, and 10 mM imidazole] by sonication. After cell lysis, the insoluble material was removed by centrifugation [27,000g (Sorvall rotor SS-34) for 30 min twice], and the supernatant was passed through a 1-ml coagarose high-performance column (GE Healthcare) pre-equilibrated with lysis buffer. The protein was washed with wash buffer [30 mM Hepes (pH 8.0), 500 mM NaCl, 10% glycerol, 2 mM mercaptoethanol, 0.02% Triton X-100, and 20 mM imidazole] and eluted with 30 mM Hepes (pH 8.0), 300 mM NaCl, 10% glycerol, 2 mM mercaptoethanol, and 200 mM imidazole. The protein was dialyzed overnight at 4°C in 4 liters dialysis buffer [50 mM tris-HCl (pH 7.5), 200 mM KCl, 25 mM MgCl$_2$, 10% g1ycerol, 1 mM DTT, and 0.1 mM EDTA] using Slide-A-Lyzer Dialysis Cassettes 3K (Thermo Fisher Scientific). The recombinant proteins were stored at −70°C. All fractions were analyzed by SDS-PAGE.

ClpP activity in isolated mitochondria
Intact mitochondria from OCI-AML2 cell lines were isolated as described above. The 1.5 μM ClpP and 4.5 μM ClpX were added to mitochondrial lysates in ClpXP protease assay buffer [25 mM tris-Cl (pH 8.0) supplemented with 3 mM adenosine triphosphate (ATP), 10 mM MgCl$_2$, 20 mM KCl, 0.03% Tween 20, 2 mM β-mercaptoethanol, 5% glycerol with an ATP regeneration system of 16 mM creatine phosphate, and creatine kinase (13 U/ml)]. This mixture was incubated for 1.5 or 3 hours at 37°C and was subjected to SDS-PAGE and BN-PAGE.

Hypoxia
Wild-type OCI-AML2 cells or OCI-AML2 cells seeded at equal cell concentrations 4 days after transduction with shRNA targeting NLN or control sequences were incubated for 48 hours under 0.2% oxygen (Hypoxygen HypOxystation H45) or 1% oxygen (Hypoxygen HypOxystation H35). For proliferation assays, cells were counted daily by trypan blue exclusion staining from days 3 to 7 after transduction.

RNA isolation and quantitative reverse transcriptase real-time polymerase chain reaction
Total RNA was isolated from AML cells using the RNeasy Plus Mini Kit (QIAGEN), and cDNA was prepared using SuperScript IV Reverse Transcriptase (Thermo Fisher Scientific). Equal amounts of cDNA for each sample were added to a prepared master mix (Power SYBR Green PCR Master mix; Applied Biosystems). Quantitative reverse transcriptase real-time polymerase chain reaction was performed on an ABI Prism 7900 sequence detection system (Applied Biosystems). The relative abundance of a transcript was represented by the threshold cycle (CT) of amplification, which is inversely correlated with the amount of target RNA/first-strand cDNA being amplified. To normalize for equal amounts of cDNA, we assayed the amounts of 18S ribosomal RNA (rRNA) gene transcript. The comparative CT was calculated as per manufacturer's instructions. Primer sequences for *NLN*-F, 5′-GGCTGAACTTGGTGCTCTTC-3′; and *NLN*-R, 5′-TAGTTTGGCCACCTTGGTTC-3′. Primer sequences for 18S rRNA-F, 5′-AGGAATTGACGGAAGGGCAC-3′; and 18S rRNA-R, 5′-GGACATCTAAGGGCATCACA-3′.

Calcium measurements
Seven days after transduction with shRNA targeting *NLN* or a control sequence, OCI-AML2 cells were stained for either the mitochondrial calcium indicator Rhod-2 AM (Thermo Fisher Scientific

Mirali *et al.*, *Sci. Transl. Med.* **12**, eaaz8264 (2020)   8 April 2020

13 of 16

R1244) or the cellular calcium indicator Fluo-8 AM (Abcam ab142773). Cells were acquired in a Fortessa cytometer (BD Biosciences), and data were analyzed with the FlowJo software (TreeStar).

8227 Flow cytometry
The 8227 cells were coimmunostained with Annexin V–FITC (BD Biosciences, BD 556419) and anti-human antibodies recognizing CD34 (BD Biosciences, BD 340411) and CD38 (Thermo Fisher Scientific 12-0388-42). Flow cytometry data were acquired using a BD Accuri flow cytometer (BD Biosciences), and frequencies of viable CD34$^+$ and CD38$^-$ cells were analyzed with the FlowJo software (TreeStar).

Xenograft models of human AML
OCI-AML2 human leukemia cells (1×10^6) were injected subcutaneously into the flanks of SCID mice. After the appearance of a palpable tumor (5 days), the mice were treated with R2 (100 mg/kg) or vehicle [10% (v/v) DMSO + 10% (v/v) cremophor + 0.9% (w/v) NaCl] intraperitoneally once daily ($n = 10$ per group) for a total of 10 days. Tumor volumes were measured three times per week based on caliper measurements of tumor length, width, and height (volume = tumor length × width × height × 0.52). At the end of treatment, mice were euthanized, and tumor volumes and mass were measured from excised tumors. Peripheral blood was collected ($n = 4$ per group), and biochemical markers of liver (aspartate transaminase, alkaline phosphatase, and bilirubin), muscle (creatine kinase), and renal (creatinine) toxicity were measured by Idexx Laboratories.

To assess R2 in mouse models of primary AML engraftment, a frozen aliquot of AML cells was thawed, counted, and resuspended in phosphate-buffered saline, and then, 2.5×10^6 viable trypan blue–negative cells were injected into the right femur of 10-week-old female NOD-SCID mice that had been irradiated with 2.08 Gy from a ^{137}Cs source and injected with 200 μg of anti-mouse CD122 24 hours previously. Similarly, engraftment of normal hematopoietic cells was assessed by the injection of 1.5×10^6 viable trypan blue–negative human cord blood cells into NOD-SCID mice. Ten days after injection of AML or human cord blood cells, mice were treated with R2 (100 mg/kg by intraperitoneal injection) or vehicle control ($n = 9$ to 10 per group) three times per week for 4 weeks. Mice were then euthanized, and the cells were flushed from the femurs using a 26-gauge needle with IMDM + 10% FBS. Engraftment of human AML cells into the marrow of the noninjected left femur was assessed by enumerating the percentage of human CD45$^+$CD33$^+$CD19$^-$ (BD Biosciences) cells by flow cytometry using the BD FACS Calibur. Data were analyzed with FlowJo version 7.7.1 (TreeStar).

To assess secondary engraftment, primary human AML cells were isolated from the bone marrow of control and R2-treated mice. Cells were pooled, and equal numbers of viable cells were transplanted into the right femur of secondary untreated mice. After 6 weeks, mice were euthanized, and human CD45$^+$CD33$^+$CD19$^-$ (BD Biosciences) cells were quantified by flow cytometry. All in vivo studies were carried out according to the regulations of the Canadian Council on Animal Care and with the approval of the University Health Network Ethics Review Board.

Statistical analysis
GraphPad Prism 6.0 was used to perform statistical analysis and data plotting. A one-way or two-way ANOVA followed by Dunnett's (one-way) or Bonferroni's (two-way) post hoc testing was used to compare mean values between multiple groups. An unpaired

Student's t test was used to compare the means between two groups. Statistical significance values were indicated as follows: *$P \leq 0.05$, **$P \leq 0.01$, ***$P \leq 0.001$, and ****$P \leq 0.0001$.

SUPPLEMENTARY MATERIALS
stm.sciencemag.org/cgi/content/full/12/538/eaaz8264/DC1
Fig. S1. Genetic knockdown of *NLN* reduces the growth of leukemic cells.
Fig. S2. Genetic knockdown of *NLN* disrupts cristae but does not alter mitochondrial mass, membrane potential, or ROS.
Fig. S3. *NLN* knockdown impairs RCS formation independently of OPA1.
Fig. S4. ClpXP degrades respiratory chain complex subunits and impairs supercomplex formation.
Fig. S5. *NLN* expression and RCS formation are down-regulated under hypoxic conditions.
Fig. S6. RCS assembly in patients with AML is not correlated with respiratory chain complex subunit expression.
Fig. S7. LETM1 complex assembly is impaired under hypoxic conditions.
Fig. S8. Genetic knockdown of *NLN* reduces LETM1 complex formation.
Fig. S9. A small-molecule inhibitor of NLN does not affect individual complex subunits.
Fig. S10. A small-molecule inhibitor of NLN reduces LETM1 complex formation.
Fig. S11. A small-molecule inhibitor of NLN reduces the growth of leukemic cells.
Fig. S12. A small-molecule inhibitor of NLN shows no evidence of toxicity in xenograft models of AML.
Table S1. Correlation of *NLN* with mutations.
Table S2. Cell lines.
Table S3. Clinical data of primary AML samples.
Data file S1. Original data.
Data file S2. Complete list of NLN's interactors identified by BioID-MS.
View/request a protocol for this paper from *Bio-protocol*.

REFERENCES AND NOTES
1. A. Cole, Z. Wang, E. Coyaud, V. Voisin, M. Gronda, Y. Jitkova, R. Mattson, R. Hurren, S. Babovic, N. Maclean, I. Restall, X. Wang, D. V. Jeyaraju, M. A. Sukhai, S. Prabha, S. Bashir, A. Ramakrishnan, E. Leung, Y. H. Qia, N. Zhang, K. R. Combes, T. Ketela, F. Lin, W. A. Houry, A. Aman, R. Al-Awar, W. Zheng, E. Wienholds, C. J. Xu, J. Dick, J. C. Wang, J. Moffat, M. D. Minden, C. J. Eaves, G. D. Bader, Z. Hao, S. M. Kornblau, B. Raught, A. D. Schimmer, Inhibition of the mitochondrial protease ClpP as a therapeutic strategy for human acute myeloid leukemia. *Cancer Cell* **27**, 864–876 (2015).
2. D. A. Pollyea, B. M. Stevens, C. L. Jones, A. Winters, S. Pei, M. Minhajuddin, A. D'Alessandro, R. Culp-Hill, K. A. Riemondy, A. E. Gillen, J. R. Hesselberth, D. Abbott, D. Schatz, J. A. Gutman, E. Purev, C. Smith, C. T. Jordan, Venetoclax with azacitidine disrupts energy metabolism and targets leukemia stem cells in patients with acute myeloid leukemia. *Nat. Med.* **24**, 1859–1866 (2018).
3. M. Skrtic, S. Sriskanthadevan, B. Jhas, M. Gebbia, X. Wang, Z. Wang, R. Hurren, Y. Jitkova, M. Gronda, N. Maclean, C. K. Lai, Y. Eberhard, J. Bartoszko, P. Spagnuolo, A. C. Rutledge, A. Datti, T. Ketela, J. Moffat, B. H. Robinson, J. H. Cameron, J. Wrana, C. J. Eaves, M. D. Minden, J. C. Wang, J. E. Dick, K. Humphries, C. Nislow, G. Giaever, A. D. Schimmer, Inhibition of mitochondrial translation as a therapeutic strategy for human acute myeloid leukemia. *Cancer Cell* **20**, 674–688 (2011).
4. S. Sriskanthadevan, D. Jeyaraju, T. Chung, S. Prabha, W. Xu, M. Skrtic, B. Jhas, R. Hurren, M. Gronda, X. Wang, Y. Jitkova, M. Sukhai, F. Lin, N. MacLean, R. Laister, C. Goard, P. Mullen, S. Xie, L. Penn, I. Rogers, J. Dick, M. Minden, A. Schimmer, AML cells have low spare reserve capacity in their respiratory chain that renders them susceptible to oxidative metabolic stress. *Blood* **125**, 2120–2130 (2015).
5. R. Anand, T. Langer, M. J. Baker, Proteolytic control of mitochondrial function and morphogenesis. *Biochim. Biophys. Acta* **1833**, 195–204 (2013).
6. J. Chabry, F. Checler, J. P. Vincent, J. Mazella, Colocalization of neurotensin receptors and of the neurotensin-degrading enzyme endopeptidase 24-16 in primary cultures of neurons. *J. Neurosci.* **10**, 3916–3921 (1990).
7. F. Checler, J. P. Vincent, P. Kitabgi, Purification and characterization of a novel neurotensin-degrading peptidase from rat brain synaptic membranes. *J. Biol. Chem.* **261**, 11274–11281 (1986).
8. V. Rioli, F. C. Gozzo, A. S. Heimann, A. Linardi, J. E. Krieger, C. S. Shida, P. C. Almeida, S. Hyslop, M. N. Eberlin, E. S. Ferro, Novel natural peptide substrates for endopeptidase 24.15, neurolysin, and angiotensin-converting enzyme. *J. Biol. Chem.* **278**, 8547–8555 (2003).
9. V. Rioli, A. Kato, F. C. V. Portaro, G. K. Cury, K. Kaat, B. Vincent, F. Checler, A. C. Camargo, M. J. Glucksman, J. L. Roberts, S. Hirose, E. S. Ferro, Neuropeptide specificity and inhibition of recombinant isoforms of the endopeptidase 3.4.24.16 family: Comparison with the related recombinant endopeptidase 3.4.24.15. *Biochem. Biophys. Res. Commun.* **250**, 5–11 (1998).

Mirali *et al.*, *Sci. Transl. Med.* **12**, eaaz8264 (2020)   8 April 2020

14 of 16

10. F. Checler, H. Barelli, P. Dauch, V. Dive, B. Vincent, J. P. Vincent, Neurolysin: Purification and asays. *Methods Enzymol.* **248**, 593–614 (1995).

11. D. M. Cavalcanti, L. M. Castro, J. C. Rosa Neto, M. Seelaender, R. X. Neves, V. Oliveira, F. L. Forti, L. K. Iwai, F. C. Gozzo, M. Todiras, I. Schadock, C. C. Barros, M. Bader, E. S. Ferro, Neurolysin knockout mice generation and initial phenotype characterization. *J. Biol. Chem.* **289**, 15426–15440 (2014).

12. V. Hung, P. Zou, H. W. Rhee, N. D. Udeshi, V. Cracan, T. Svinkina, S. A. Carr, V. K. Mootha, A. Y. Ting, Proteomic mapping of the human mitochondrial intermembrane space in live cells via ratiometric APEX tagging. *Mol. Cell* **55**, 332–341 (2014).

13. H. W. Rhee, P. Zou, N. D. Udeshi, J. D. Martell, V. K. Mootha, S. A. Carr, A. Y. Ting, Proteomic mapping of mitochondria in living cells via spatially restricted enzymatic tagging. *Science* **339**, 1328–1331 (2013).

14. P. F. Teixeira, G. Masuyer, C. M. Pinho, R. M. M. Branca, B. Kmiec, C. Wallin, S. K. T. S. Warmlander, R. P. Berntsson, M. Ankarcrona, A. Graslund, J. Lehtio, P. Stenmark, E. Glaser, Mechanism of peptide binding and cleavage by the human mitochondrial peptidase neurolysin. *J. Mol. Biol.* **430**, 348–362 (2018).

15. E. Lapuente-Brun, R. Moreno-Loshuertos, R. Acín-Pérez, A. Latorre-Pellicer, C. Colás, E. Balsa, E. Perales-Clemente, P. M. Quirós, E. Calvo, M. A. Rodríguez-Hernández, P. Navas, R. Cruz, A. Carracedo, C. López-Otín, A. Pérez-Martos, P. Fernández-Silva, E. Fernández-Vizarra, J. A. Enríquez, Supercomplex assembly determines electron flux in the mitochondrial electron transport chain. *Science* **340**, 1567–1570 (2013).

16. C. Bianchi, M. L. Genova, G. Parenti Castelli, G. Lenaz, The mitochondrial respiratory chain is partially organized in a supercomplex assembly: Kinetic evidence using flux control analysis. *J. Biol. Chem.* **279**, 36562–36569 (2004).

17. C. Greggio, P. Jha, S. S. Kulkarni, S. Lagarrigue, N. T. Broskey, M. Boutant, X. Wang, S. Conde Alonso, E. Ofori, J. Auwerx, C. Canto, F. Amati, Enhanced respiratory chain supercomplex formation in response to exercise in human skeletal muscle. *Cell Metab.* **25**, 301–311 (2017).

18. S. W. Ng, A. Mitchell, J. A. Kennedy, W. C. Chen, J. McLeod, N. Ibrahimova, A. Arruda, A. Popescu, V. Gupta, A. D. Schimmer, A. C. Schuh, K. W. Yee, L. Bullinger, T. Herold, D. Gorlich, T. Buchner, W. Hiddemann, W. E. Berdel, B. Wormann, M. Cheok, C. Preudhomme, H. Dombret, K. Metzeler, C. Buske, B. Lowenberg, P. J. Valk, P. W. Zandstra, M. D. Minden, J. E. Dick, J. C. Wang, A 17-gene stemness score for rapid determination of risk in acute leukaemia. *Nature* **540**, 433–437 (2016).

19. J. K. Warner, J. C. Wang, K. Takenaka, S. Doulatov, J. L. McKenzie, L. Harrington, J. E. Dick, Direct evidence for cooperating genetic events in the leukemic transformation of normal human hematopoietic cells. *Leukemia* **19**, 1794–1805 (2005).

20. S. Tamai, H. Iida, S. Yokota, T. Sayano, S. Kiguchiya, N. Ishihara, J. Hayashi, K. Mihara, T. Oka, Characterization of the mitochondrial protein LETM1, which maintains the mitochondrial tubular shapes and interacts with the AAA-ATPase BCS1L. *J. Cell Sci.* **121**, 2588–2600 (2008).

21. D. Jiang, L. Zhao, D. E. Clapham, Genome-wide RNAi screen identifies Letm1 as a mitochondrial Ca^{2+}/H^+ antiporter. *Science* **326**, 144–147 (2009).

22. C. S. Hines, K. Ray, J. J. Schmidt, F. Xiong, R. W. Feenstra, M. Pras-Raves, J. P. de Moes, J. H. Lange, M. Melikishvili, M. G. Fried, P. Mortenson, M. Charlton, Y. Patel, S. M. Courtney, C. G. Kruse, D. W. Rodgers, Allosteric inhibition of the neuropeptidase neurolysin. *J. Biol. Chem.* **289**, 35605–35619 (2014).

23. E. R. Lechman, B. Gentner, S. W. Ng, E. M. Schoof, P. van Galen, J. A. Kennedy, S. Nucera, F. Ciceri, K. B. Kaufmann, N. Takayama, S. M. Dobson, A. Trotman-Grant, G. Krivdova, J. Elzinga, A. Mitchell, B. Nilsson, K. G. Hermans, K. Eppert, R. Marke, R. Isserlin, V. Voisin, G. D. Bader, P. W. Zandstra, T. R. Golub, B. L. Ebert, J. Lu, M. Minden, J. C. Wang, L. Naldini, J. E. Dick, miR-126 regulates distinct self-renewal outcomes in normal and malignant hematopoietic stem cells. *Cancer Cell* **29**, 214–228 (2016).

24. A. Serizawa, P. M. Dando, A. J. Barrett, Characterization of a mitochondrial metallopeptidase reveals neurolysin as a homologue of thimet oligopeptidase. *J. Biol. Chem.* **270**, 2092–2098 (1995).

25. C. R. Hackenbrock, B. Chazotte, S. S. Gupte, the random collision model and a critical assessment of diffusion and collision in mitochondrial electron transport. *J. Bioenerg. Biomembr.* **18**, 331–368 (1986).

26. H. Schagger, K. Pfeiffer, Supercomplexes in the respiratory chains of yeast and mammalian mitochondria. *EMBO J.* **19**, X177–X1783 (2000).

27. J. A. Letts, K. Fiedorczuk, L. A. Sazanov, The architecture of respiratory supercomplexes. *Nature* **537**, 644–648 (2016).

28. R. Acin-Perez, J. A. Enriquez, The function of the respiratory supercomplexes: The plasticity model. *Biochim. Biophys. Acta* **1837**, 444–450 (2014).

29. J. A. Letts, L. A. Sazanov, Clarifying the supercomplex: The higher-order organization of the mitochondrial electron transport chain. *Nat. Struct. Mol. Biol.* **24**, 800–808 (2017).

30. E. Maranzana, G. Barbero, A. I. Falasca, G. Lenaz, M. L. Genova, Mitochondrial respiratory supercomplex association limits production of reactive oxygen species from complex I. *Antioxid. Redox Signal.* **19**, 1469–1480 (2013).

31. I. Lopez-Fabuel, J. Le Douce, A. Logan, A. M. James, G. Bonvento, M. P. Murphy, A. Almeida, J. P. Bolanos, Complex I assembly into supercomplexes determines differential mitochondrial ROS production in neurons and astrocytes. *Proc. Natl. Acad. Sci. U.S.A.* **113**, 13063–13068 (2016).

32. H. Schagger, R. de Coo, M. F. Bauer, S. Hofmann, C. Godinot, U. Brandt, Significance of respirasomes for the assembly/stability of human respiratory chain complex I. *J. Biol. Chem.* **279**, 36349–36353 (2004).

33. R. Acin-Perez, M. P. Bayona-Bafaluy, P. Fernandez-Silva, R. Moreno-Loshuertos, A. Perez-Martos, C. Bruno, C. T. Moraes, J. A. Enriquez, Respiratory complex III Is required to maintain complex I in mammalian mitochondria. *Mol. Cell* **13**, 805–815 (2004).

34. S. Cogliati, E. Calvo, M. Loureiro, A. M. Guaras, R. Nieto-Arellano, C. Garcia-Poyatos, I. Ezkurdia, N. Mercader, J. Vazquez, J. A. Enriquez, Mechanism of super-assembly of respiratory complexes III and IV. *Nature* **539**, 579–582 (2016).

35. S. Cogliati, C. Frezza, M. E. Soriano, T. Varanita, R. Quintana-Cabrera, M. Corrado, S. Cipolat, V. Costa, A. Casarin, L. C. Gomes, E. Perales-Clemente, L. Salviati, P. Fernandez-Silva, J. A. Enriquez, L. Scorrano, Mitochondrial cristae shape determines respiratory chain supercomplexes assembly and respiratory efficiency. *Cell* **155**, 160–171 (2013).

36. E. G. Williams, Y. Wu, P. Jha, S. Dubuis, P. Blattmann, C. A. Argmann, S. M. Houten, T. Amariuta, W. Wolski, N. Zamboni, R. Aebersold, J. Auwerz, Systems proteomics of liver mitochondria function. *Science* **352**, aad0189 (2016).

37. K. S. Dimmer, F. Navoni, A. Casarin, E. Trevisson, S. Endele, A. Winterpacht, L. Salviati, L. Scorrano, LETM1, deleted in Wolf-Hirschhorn syndrome is required for normal mitochondrial morphology and cellular viability. *Hum. Mol. Genet.* **17**, 201–214 (2008).

38. E. D. Lagadinou, A. Sach, K. Callahan, R. M. Rossi, S. J. Neering, M. Minhajuddin, J. M. Ashton, S. Pei, V. Grose, K. M. O'Dwyer, J. L. Liesveld, P. S. Brookes, M. W. Becker, C. T. Jordan, BCL-2 inhibition targets oxidative phosphorylation and selectively eradicates quiescent human leukemia stem cells. *Cell Stem Cell* **12**, 329–341 (2013).

39. T. Haferlach, A. Kohlmann, L. Wieczorek, G. Basso, G. T. Kronnie, M. C. Bene, J. De Vos, J. M. Hernandez, W. K. Hofmann, K. I. Mills, A. Gilkes, S. Chiaretti, S. A. Shurtleff, T. J. Kipps, L. Z. Rassenti, A. E. Yeoh, P. R. Papenhausen, W. M. Liu, P. M. Williams, R. Foa, Clinical utility of microarray-based gene expression profiling in the diagnosis and subclassification of leukemia: Report from the International Microarray Innovations in Leukemia Study Group. *J. Clin. Oncol.* **28**, 2529–2537 (2010).

40. J. W. Tyner, C. E. Tognon, D. Bottomly, B. Wilmot, S. E. Kurtz, S. L. Savage, N. Long, A. R. Schultz, E. Traer, M. Abel, A. Agarwal, A. Blucher, U. Borate, J. Bryant, R. Burke, A. Carlos, R. Carpenter, J. Carroll, B. H. Chang, C. Coblentz, A. d'Almeida, R. Cook, A. Danilov, K. T. Dao, M. Degnin, D. Devine, J. Dibb, D. K. t. Edwards, C. A. Eide, I. English, J. Glover, R. Henson, H. Ho, A. Jemal, K. Johnson, R. Johnson, B. Junio, A. Kaempf, J. Leonard, C. Lin, S. Q. Liu, P. Lo, M. M. Loriaux, S. Luty, T. Macey, J. MacManiman, J. Martinez, M. Mori, D. Nelson, C. Nichols, J. Peters, J. Ramsdill, A. Rofelty, R. Schuff, R. Searles, E. Segerdell, R. L. Smith, S. E. Spurgeon, T. Sweeney, A. Thapa, C. Visser, J. Wagner, K. Watanabe-Smith, K. Werth, J. Wolf, L. White, A. Yates, H. Zhang, C. R. Cogle, R. H. Collins, D. C. Connolly, M. W. Deininger, L. Drusbosky, C. S. Hourigan, C. T. Jordan, P. Kropf, T. L. Lin, M. E. Martinez, B. C. Medeiros, R. R. Pallapati, D. A. Pollyea, R. T. Swords, J. M. Watts, S. J. Weir, D. L. Wiest, R. M. Winters, S. K. McWeeney, B. J. Druker, Functional genomic landscape of acute myeloid leukaemia. *Nature* **562**, 526–531 (2018).

41. F. E. Nicolini, J. D. Cashman, D. E. Hogge, R. K. Humphries, C. J. Eaves, NOD/SCID mice engineered to express human IL-3, GM-CSF and Steel factor constitutively mobilize engrafted human progenitors and compromise human stem cell regeneration. *Leukemia* **18**, 341–347 (2004).

42. E. Coyaud, M. Mis, E. Laurent, W. Dunham, A. L. Couzens, M. Robitaille, A. C. Gingras, S. Angers, B. Raught, BioID-based Identification of Skp Cullin F-box (SCF)β-TrCP1/2 E3 Ligase Substrates. *Mol. Cell. Proteomics* **14**, 1781–1795 (2015).

43. D. Kessner, M. Chambers, R. Burke, D. Agus, P. Mallick, ProteoWizard: Open source software for rapid proteomics tools development. *Bioinformatics* **24**, 2534–2536 (2008).

44. R. Craig, R. C. Beavis, TANDEM: Matching proteins with tandem mass spectra. *Bioinformatics* **20**, 1466–1467 (2004).

45. J. K. Eng, T. A. Jahan, M. R. Hoopmann, Comet: An open-source MS/MS sequence database search tool. *Proteomics* **13**, 22–24 (2013).

46. G. Teo, G. Liu, J. Zhang, A. I. Nesvizhskii, A. C. Gingras, H. Choi, SAINTexpress: Improvements and additional features in significance analysis of INTeractome software. *J. Proteome* **100**, 37–43 (2014).

47. H. Choi, B. Larsen, Z. Y. Lin, A. Breitkreutz, D. Mellacheruvu, D. Fermin, Z. S. Qin, M. Tyers, A. C. Gingras, A. I. Nesvizhskii, SAINT: Probabilistic scoring of affinity purification-mass spectrometry data. *Nat. Methods* **8**, 70–73 (2011).

48. A. Perelman, C. Wachtel, M. Cohen, S. Haupt, H. Shapiro, A. Tzur, JC-1: Alternative excitation wavelengths facilitate mitochondrial membrane potential cytometry. *Cell Death Dis.* **3**, e430 (2012).

49. S. G. Kang, M. R. Maurizi, M. Thompson, T. Mueser, B. Ahvazi, Crystallography and mutagenesis point to an essential role for the N-terminus of human mitochondrial ClpP. *J. Struct. Biol.* **148**, 338–352 (2004).

Mirali *et al.*, *Sci. Transl. Med.* **12**, eaaz8264 (2020)   8 April 2020

15 of 16

50. M. S. Kimber, A. Y. Yu, M. Borg, E. Leung, H. S. Chan, W. A. Houry, Structural and theoretical studies indicate that the cylindrical protease ClpP samples extended and compact conformations. *Structure* **18**, 798–808 (2010).

51. K. S. Wong, M. F. Mabanglo, T. V. Seraphim, A. Mollica, Y. Q. Mao, K. Rizzolo, E. Leung, M. T. Moutaoufik, L. Hoell, S. Phanse, J. Goodreid, L. R. S. Barbosa, C. H. I. Ramos, M. Babu, V. Mennella, R. A. Batey, A. D. Schimmer, W. A. Houry, Acyldepsipeptide analogs dysregulate human mitochondrial clpp protease activity and cause apoptotic cell death. *Cell Chem. Biol.* **25**, 1017–1030 (2018).

52. C. D. Lee, H. C. Sun, S. M. Hu, C. F. Chiu, A. Homhuan, S. M. Liang, C. H. Leng, T. F. Wang, An improved SUMO fusion protein system for effective production of native proteins. *Protein Sci.* **17**, 1241–1248 (2008).

Citation: S. Mirali, A. Botham, V. Voisin, C. Xu, J. St-Germain, D. Sharon, F. W. Hoff, Y. Qiu, R. Hurren, M. Gronda, Y. Jitkova, B. Nachmias, N. MacLean, X. Wang, A. Arruda, M. D. Minden, T. M. Horton, S. M. Kornblau, S. M. Chan, G. D. Bader, B. Raught, A. D. Schimmer, The mitochondrial peptidase, neurolysin, regulates respiratory chain supercomplex formation and is necessary for AML viability. *Sci. Transl. Med.* **12**, eaaz8264 (2020).

Mirali *et al.*, *Sci. Transl. Med.* **12**, eaaz8264 (2020)   8 April 2020

16 of 16

Science Translational Medicine

The mitochondrial peptidase, neurolysin, regulates respiratory chain supercomplex formation and is necessary for AML viability

Sara Mirali, Aaron Botham, Veronique Voisin, Changjiang Xu, Jonathan St-Germain, David Sharon, Fieke W. Hoff, Yihua Qiu, Rose Hurren, Marcela Gronda, Yulia Jitkova, Boaz Nachmias, Neil MacLean, Xiaoming Wang, Andrea Arruda, Mark D. Minden, Terzah M. Horton, Steven M. Kornblau, Steven M. Chan, Gary D. Bader, Brian Raught and Aaron D. Schimmer

Cutting leukemia's energy supply

Neurolysin is a protein that is found in the mitochondria and secreted into the circulation. It is known to help regulate physiological functions such as blood pressure but is not essential for survival in mice. Mirali *et al.* discovered that neurolysin is frequently overexpressed in acute myeloid leukemia. The authors examined the underlying mechanism and identified the role of neurolysin in the formation of respiratory chain supercomplexes in the mitochondria. They also showed that inhibition of neurolysin is selectively toxic to leukemic cells without affecting normal hematopoietic cells and demonstrated the effectiveness of this approach in mouse models of leukemia.

ARTICLE TOOLS	http://stm.sciencemag.org/content/12/538/eaaz8264
SUPPLEMENTARY MATERIALS	http://stm.sciencemag.org/content/suppl/2020/04/06/12.538.eaaz8264.DC1
RELATED CONTENT	http://stm.sciencemag.org/content/scitransmed/11/516/eaax2863.full http://stm.sciencemag.org/content/scitransmed/11/508/eaaw8828.full http://stm.sciencemag.org/content/scitransmed/10/431/eaam8460.full http://stm.sciencemag.org/content/scitransmed/12/538/eaax5104.full
REFERENCES	This article cites 52 articles, 17 of which you can access for free http://stm.sciencemag.org/content/12/538/eaaz8264#BIBL
PERMISSIONS	http://www.sciencemag.org/help/reprints-and-permissions

Use of this article is subject to the Terms of Service